SECURITY CLASSIFICATION OF THIS PAGE *(When Data Entered)*

REPORT DOCUMENTATION PAGE		READ INSTRUCTIONS BEFORE COMPLETING FORM
1. REPORT NUMBER NAVENVPREDRSCHFAC Contractor Report CR 84-07	2. GOVT ACCESSION NO.	3. RECIPIENT'S CATALOG NUMBER
4. TITLE *(and Subtitle)* Diagnostic Aids and Analyses for Smaller-Scale Moisture Structure		5. TYPE OF REPORT & PERIOD COVERED Final
		6. PERFORMING ORG. REPORT NUMBER
7. AUTHOR(s) John J. Cahir, Gregory S. Forbes, Walter D. Lottes		8. CONTRACT OR GRANT NUMBER(s) N00014-80-C-0954
9. PERFORMING ORGANIZATION NAME AND ADDRESS Department of Meteorology The Pennsylvania State University University Park, PA 16802		10. PROGRAM ELEMENT, PROJECT, TASK AREA & WORK UNIT NUMBERS PE 61153N PN WF59-551 NEPRF WU 6.2-3
11. CONTROLLING OFFICE NAME AND ADDRESS Naval Air Systems Command Department of the Navy Washington, DC 20361		12. REPORT DATE October 1984
		13. NUMBER OF PAGES 100
14. MONITORING AGENCY NAME & ADDRESS*(If different from Controlling Office)* Naval Environmental Prediction Research Facility Monterey, CA 93943		15. SECURITY CLASS. *(of this report)* UNCLASSIFIED
		15a. DECLASSIFICATION/DOWNGRADING SCHEDULE

16. DISTRIBUTION STATEMENT *(of this Report)*

Approved for public release; distribution is unlimited.

17. DISTRIBUTION STATEMENT *(of the abstract entered in Block 20, If different from Report)*

18. SUPPLEMENTARY NOTES

19. KEY WORDS *(Continue on reverse side if necessary and identify by block number)*

Cyclogenesis
Low-level jet
Jet stream
Moist conveyor belt

Polar lows
Interactive analysis
Short range forecasting

20. ABSTRACT *(Continue on reverse side if necessary and identify by block number)*

   A model of the disturbed area sometimes found ahead of cold fronts in association with a low-level and upper-level jet is described. Use of the term "moist conveyor belt" to describe this feature is suggested. A method for recognizing the feature with associated attributes also is described.
   Polar lows and means of identifying synoptic scale environmental factors related to their development are an additional topic considered.

((continued on reverse))

DD ₁ FORM 1473   EDITION OF 1 NOV 65 IS OBSOLETE
  1 JAN 73
S/N 0102-014-6601

Block 20, Abstract, continued.

Means of objectively locating air mass boundaries are developed along with an objective aid in short term prediction of heavy rain.

The report suggests that short range forecasting is limited by inadequate moisture observations, and that a major effort is needed to upgrade data availability in that area.

AB (27)   An atmosphere model of the disturbed area sometimes
          found ahead of cold fronts in association with a
          low-level and upper-level jet is described. Use of the
          term 'moist conveyor belt' to describe this feature is
          suggested and a method for recognizing the feature with
          associated attributes is described. Polar lows and
          means of identifying synoptic scale environmental
          factors related to their development are also
          considered. Means of objectively locating air mass
          boundaries are devloped along with and objective aid in
          short term prediction of heavy rain. The report
          suggests that short range forecasting is limited by
          inadequate moisture observations, and that a major
          effort is needed to upgrade data availability in that
          area. Keywords: Weather forecasting; Short time range;
          Small space scales; Humidity; Clouds; Moist conveyor
          belt weather models; Cyclogenesis; Low-level jet; Jet
          stream; Polar lows; Computerized simulation;
          Interactive analysis; Air mass analysis.

NAVENVPREDRSCHFAC CR 84-07

DIAGNOSTIC AIDS AND ANALYSES FOR SMALLER-SCALE MOISTURE STRUCTURE

Prepared By:

John J. Cahir, Gregory S. Forbes, Walter D. Lottes
Meteorology Department, The Pennsylvania State University
University Park, PA 16802

Contract No. N00014-80-C-0954

OCTOBER 1984

APPROVED FOR PUBLIC RELEASE; DISTRIBUTION IS UNLIMITED

Prepared For:
NAVAL ENVIRONMENTAL PREDICTION RESEARCH FACILITY
MONTEREY, CALIFORNIA 93943

Table of Contents

List of Figures

List of Figures

iv

Summary

This is the final report on a project which proposed the following:

1. To develop new means of estimating humidity in disturbed (cloudy) regions for application to short-range forecasting of smaller (than synoptic) scale hydrometeors. We have developed and tested a humidity (and wind) model of the moist conveyor belt, an important precipitation and cloudiness-producing flow sometimes found ahead of cold fronts. Findings include a recognition method, a favored region for deep layers of high humidity, evidence that embedded convection may be mislocated in the literature, a favored location for a low-level jet and for a cyclonic disturbance and associated front that apparently move with the belt. Computer programs for application are available. See Chapter 2. A thesis by Thaddeus Staskiewicz gives more details.

2. To identify factors differentiating stronger polar lows from weak ones. We have found that the magnitude of the pressure disturbance associated with polar lows can be estimated quite well from satellite imagery, and have identified synoptic scale environment factors related to developing polar lows: large low-level vorticity and steep lapse rates (but the underlying ocean is cold, because these features occur at high latitudes. See Chapter 3). Two papers by Forbes and Lottes and Forbes and Merritt provide more detail.

3. To develop methods of objectively locating subtle regions that may become meteorologically active. We have adapted and tested an objective boundary locator, analogous to $GG\theta$, for locating moisture and temperature boundaries, using wet bulb potential temperature; forecasting experiments and composite heavy precipitation patterns related to convergence on these

boundaries are described in Chapter 4. A thesis by Arthur Person provides more detail.

4. To conduct a planning effort for a more elaborate series of field experiments. This part of the project was not successful. We visited a Fleet Oceanographic Facility (NORVA) and held discussions in Monterey and Seattle. However, the lack of data to verify hypotheses and tests over the oceans proved to inhibit these plans.

5. To adapt existing and developing computer programs for interactive analysis of conventional meteorological data on minicomputer systems. Numerous such programs were installed and are available in the SPADS Eclipse minicomputer. See our first project report.

Much of the work reported here relates to the perplexing problem of inferring the behavior the moisture field--the object of many weather forecasts--for application over short time ranges and small space scales. Many, if not most, interesting forecasting situations occur in cloudy regions, where current and most proposed remote sensing techniques fail. Thus, our model of the moist conveyor belt, which was developed over land, reveals some details of its wind and humidity structure. If it can be applied in a cloudy region over the ocean, it could provide some smaller than synoptic-scale information that is otherwise not available.

We have developed and tested a technique for diagnosing, locating and displaying potentially active surface boundaries, and tested its application in real-time conditions. These tests showed that forecasters could produce high quality forecasts with or without the boundary locator, but it was not clear whether they had learned how to do it from the use of the computer system. In any case, their forecasts were excellent. We also performed a pilot study to produce an objective aid in short term prediction of strong

rains. This relies heavily on the flux divergence of surface water vapor. Also, we have identified a method of classifying polar lows and recognizing conditions favorable for their growth.

All of these approaches can generate only very small gains in forecasting skill over land, at best. The situation could be different over the ocean. They do suggest that much can be done over the next few years, as mesoscale wind observations become available. The work also suggests that short-range forecasting is limited by inadequate moisture observations and that a major effort is needed in that area.

I. Introduction

1. Background

This project has been directed toward better use of available observations to improve short-range weather prediction. Special emphasis has been placed on the moisture field, because moisture is of critical interest to forecasters and because the small horizontal scale of many moisture features results in their relatively poorer specifications and prediction in numerical models than in the case for the mass field. Much of the developmental work has been carried out over land, but it is believed that the principles apply over the oceans, as well. Accordingly, during the period covered by the present report, work has been completed on three moisture-related applications: (1) Development of a vertically consistent humidity/wind model of significant poleward flows that produce extensive clouds and precipitation, called conveyor belts. (2) Identification of the differences in some larger scale parameters which may govern the development, or lack of thereof, of vigorous small-scale cloud clusters over the high latitude oceans, called polar lows. (3) Location of critical moisture and temperature boundaries which may become meteorologically active. In the case of active boundaries, case studies were performed and summarized and a forecasting experiment was conducted in real time. All of these appear to have application to the meteorological problems encountered by the Navy.

2. Previous work

During the first year of the Naval Environmental Prediction Research Facility (NEPRF) Grant No. N00014-80-C-0954, two major activities took place. These were reported on in the report entitled "Diagnostic Aids and Analyses for Smaller Scale Moisture Structure dated October 1981. One activity was

the development of computer programs suitable for real-time analysis, and the other was a research thrust toward obtaining better moisture analyses.

Several computer programs, reflecting research and development work in analysis and short-range prediction conducted at Penn State for several years, were modified and adapted to the Eclipse S250 (SPADS) minicomputer and its operating system. These programs for analysis and diagnosis are up and running at the SPADS facility. Documentation for new programs was included in the previous report. Instruction in the use of programs is available in that report and in this one. Other information is available at the Penn State Meteorology Laboratory.

The second activity has been research directed toward finding better methods of analyzing moisture fields in data-poor regions, notably over the oceans. However, instead of a general approach, such as that taken by other investigators interested in remote sensing, the emphasis of this work was on disturbed parts of the atmosphere, where most of the interesting weather takes place. The reason for this emphasis lies on the frequent use of moisture analyses, such as moisture convergence, in our forecasting procedures. Thus, we need good moisture fields in and around cyclones, frontal bands, jet streams and the like, and are less sensitive to the accuracy and quality in dry regions. Unfortunately, it is in cloudy places that remotely-sensed humidity analyses are often poorest, especially over the oceans.

Accordingly, we have worked with the "conveyor belt" (Browning and Harrold, 1969). A conveyor belt is a flow of warm, moist, rather cloudy air flowing poleward and upward. It is often part of a cyclonic system, and it is a major precipitation-producer (Carlson, 1980). It also has some very interesting substructures, such as imbedded mesoscale bands, that are of critical importance to forecasters.

Using radiosonde data in regions of satisfactory data coverage, we initially developed a non-dimensional relative humidity model of the conveyor belt. The model permits one to make estimates of the relative humidity at various points in and near the belt. The humidity model is discussed in the first report, but it had not been tested or generalized to produce wind estimates. That testing and the development of a wind model, plus other work involving humidity features over oceans, location of meteorologically active boundaries and some tests of the utility of these products, is presented in this report.

3. Organization of present report

The relative humidity model of the conveyor belt has been refined and tested on independent data during the current year. In addition, a wind field model of the belt has also been developed. The wind model has been checked for synoptic consistency with the humidity model by calculation of model vorticity and wind shears and location of wind maxima. These fields, which can be thought of as being independent of each other, both point strongly to a favored location for cyclonic activity under the belt as well as for front location. Inasmuch as a numerical model could recover a consistent thermal field from these winds, it would be possible, over the ocean, to enter into a numerical prediction model a mutually consistent wind and humidity field at a horizontal resolution of about 100 km in a region of important cloudiness and precipitation, based on a single satellite image. This work is described in Chapter II.

Another important weather feature over the ocean is the polar low (Reed, 1979; Rasmussen, 1979). This is a cloud cluster of less-than-synoptic scale that forms with a frequency of order 1 day^{-1} over high latitude oceans in

winter. It typically grows to the detection level in the surface pressure pattern and can deepen to become a respectable, though usually small, cyclone. Heavy weather is a normal feature of polar lows. In Chapter III, the conditions in which polar lows form over the Atlantic are studied and summarized. These studies show that developing polar lows are favored in high vorticity, unstable regions. This suggests that potential vorticity analyses and predictions on an appropriate scale may be of considerable value in anticipating the development and behavior of these dangerous structures.

Chapter IV presents work in locating potentially meteorologically active boundaries. Sometimes these coincide with front locations, but the objective is to develop a technique that is applicable to mesoscale boundaries, especially moisture boundaries. The latter often do not satisfy the criteria for front location, but can be sites of important convective systems (Purdom, 1976). The technique used is an extension of that of Clarke and Renard (1966), adapted to weak thermal boundaries featuring moisture contrast. The method appears to be ready to test on finer scale mesoscale structures, as mesoscale observations become available. A test on the scale for which observations are available (meso-α scale at the surface, and synoptic scale aloft) was performed under the contract, and is described in Chapter IV.

II. The Warm Conveyor Belt - A Consistent Wind/Humidity Model for Possible Application over Oceans.

1. Introduction

Conveyor belts have been mentioned in literature since the introduction of the term by Browning (1971) and Harrold (1973). In apparent analogy to the industrial device, what was originally visualized was a flow of air ascending from a moist source region, delivering a volume of warm moist air to the higher troposphere over middle and high latitudes. Such belts are sometimes observed in association with eastward-progressing cold fronts in middle and high latitudes. They can be important sources of precipitation. Other authors (Carlson, 1980) have extended the concept of the conveyor belt to other types of ascending or descending currents, including dry or cold flows. In all of those papers the belts in question are of synoptic scale, not flows into cumulus convection; their time scale is of the order of a day or two. A restriction in the present case is that only the warm conveyor belt is considered, although its interaction with a dry belt is mentioned.

In particular, this research is directed toward determining favored regions for smaller-scale wind and humidity features within the typical warm conveyor belt. A composite model, based on radiosonde observations of wind and humidity is developed in a curving, non-dimensionalized coordinate system centered on the belt. Thirty-eight cases were used to develop the model, with independent tests performed on 23 later cases. Data for all cases were observed over the eastern United States. Features such as the Appalachians, the eastern coast of North America, the Great Lakes, and the position of the radiosonde network relative to the region of maximum cyclogenesis and poleward eddy flux off the coast may give a local bias to the model. Conveyor belts can be seen in satellite pictures elsewhere, but may have different

5

properties. However, to the extent that large-scale dynamical features are involved, limited application of the model elsewhere may be possible.

The warm conveyor belt typically involves warm advection and winds veering upward. Air trajectories tend to be anticyclonically curved in the circumstances. Accordingly, the discussion is limited to conveyor belts that curve anticyclonically in infrared satellite imagery. A further restriction is that the belt have a sharp left (cold side) edge from the point of view of an observer looking downwind. These restrictions eliminate consideration of belts which spiral cyclonically into well-developed and mature cyclones as well as of moist pre-frontal cloud bands which may be conveyor belts, but which lack a well-defined left edge. More-or-less east-west cloud bands are avoided and cold or dry belts are also excluded. Well-developed cyclones, especially of the cut-off variety may distort the appearance of the conveyor belt, imparting cyclonic curvature to it. Those cases were excluded from the present work. Also, cirrus shields similar in appearance to the top of conveyor belts sometimes occur and should be distinguished from conveyor belts when possible. Examples are jet stream cirrus (Oliver, et al., 1964), the baroclinic leaf (Weldon, 1979), and blowoff from mesoscale convective complexes (Maddox, 1980).

Overall, the objective is to concentrate on a class of belts that can be reasonably consistently identified by inspection of satellite images. To the extent that the model is valid in regions of no radiosondes, some estimates of wind and humidity distribution might be obtained in cloudy regions, which are problematical from the point of view of most remote sensing methods, but are of intense interest to operational meteorologists.

It was possible to identify 61 warm conveyor belts over the eastern United States during 1978-1982. They are less common in summer than in colder

6

seasons when cold air is more available to be overrun. Assuming that conditions favorable for sharp, anticyclonically turning belts are occasionally found east of 3 or 4 major upper trough positions, and allowing for about 50% underdetection in our sample, the implied frequency for the Northern Hemisphere should be about one such belt every 3 or 4 days. Similar structures appear in Southern Hemisphere imagery.

In section 2, some synoptic characteristics of warm conveyor belts are reviewed. A method of identifying suitable belts from satellite imagery and of compositing the associated radiosonde data in a non-dimensional coordinate is described in section 3. Section 4 presents the composite wind and humidity analyses at low, middle, and upper levels of the conveyor, followed in section 5 by comparison to an independent sample.

2. Synoptic features of conveyor belts

The warm conveyor belt is usually found ahead of, or over, eastward-moving cold fronts in middle and high latitudes, but identification from satellite imagery does not require any knowledge of front location or existence. Instead the air is cloudy with cold tops, recognizable in the pictures. Figs. 1-3 show an example of enhanced infrared imagery of a belt on 24 November 1980, together with the associated surface and 300 mb charts, three hours earlier. The anticyclonically curved sharp left edge attracts the eye, and is the key feature for identifying and locating the belt. Note in Fig. 2 that extensive precipitation is occurring in the region of cold-topped clouds (the conveyor belt) that extends from the FL panhandle northeastward over NC, PA, to ME. Rainfall amounts of 20 mm or more were reported along a zone from Jacksonville, FL to Eastport, ME over the succeeding 24 h. The surface frontal analysis for 1200 GMT 24 November, taken directly from the
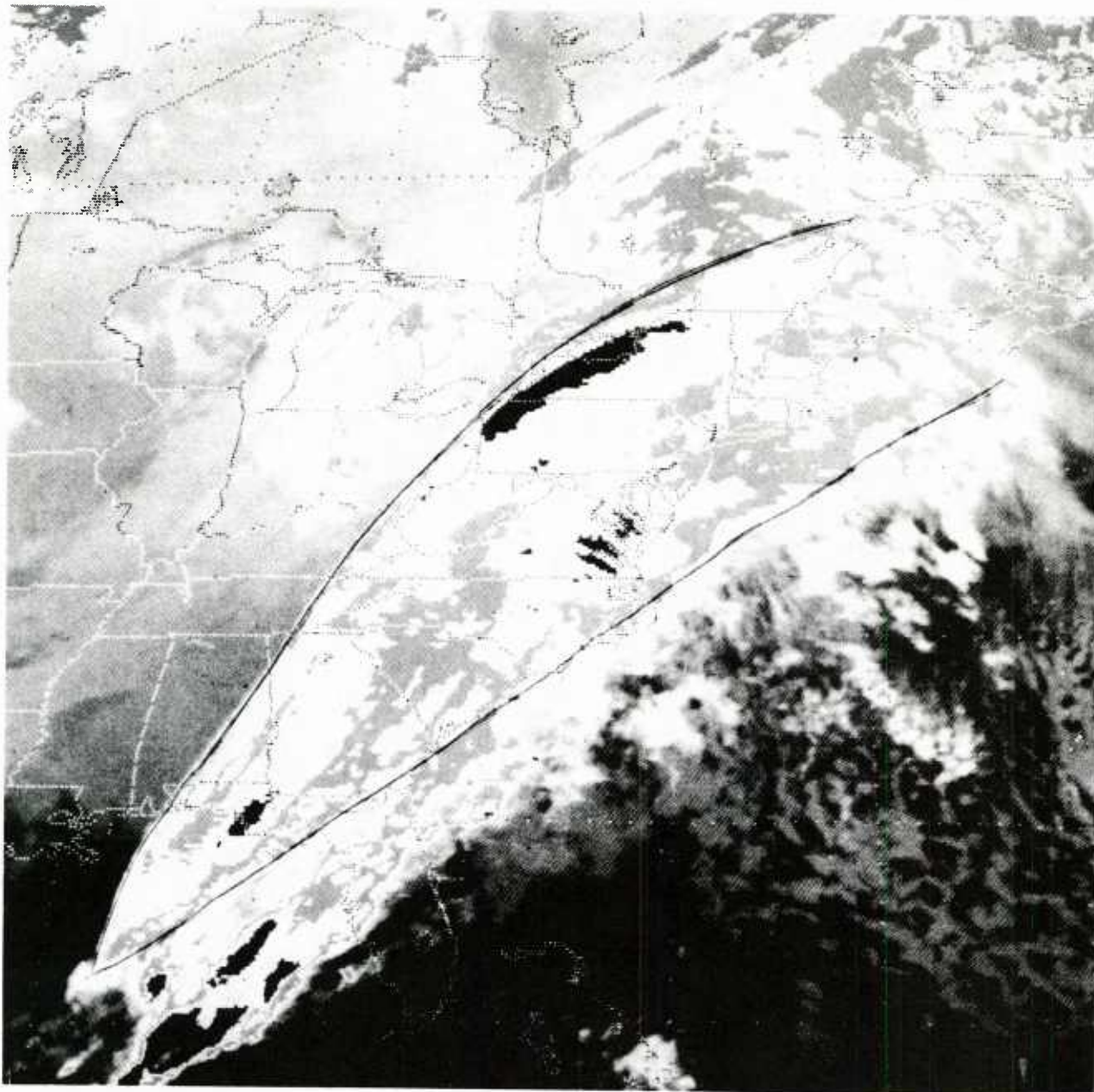
Figure 1.   Enhanced (MB) infrared satellite image of a conveyor belt
             over the eastern United States, 24 Nov 1980, 1500 GMT.

8
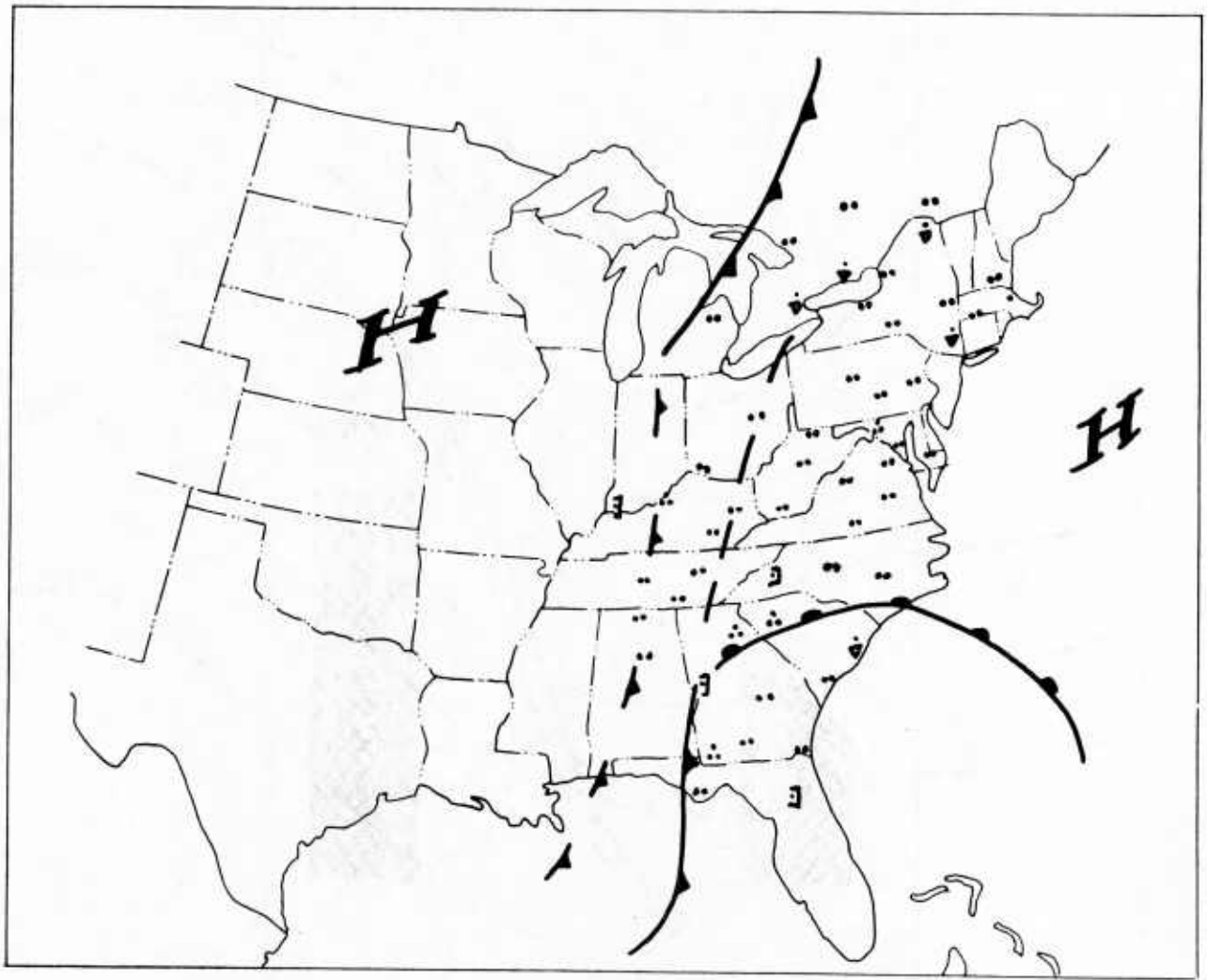
Figure 2.   Elements of the sea-level chart, 24 Nov 1980, 1200 GMT.
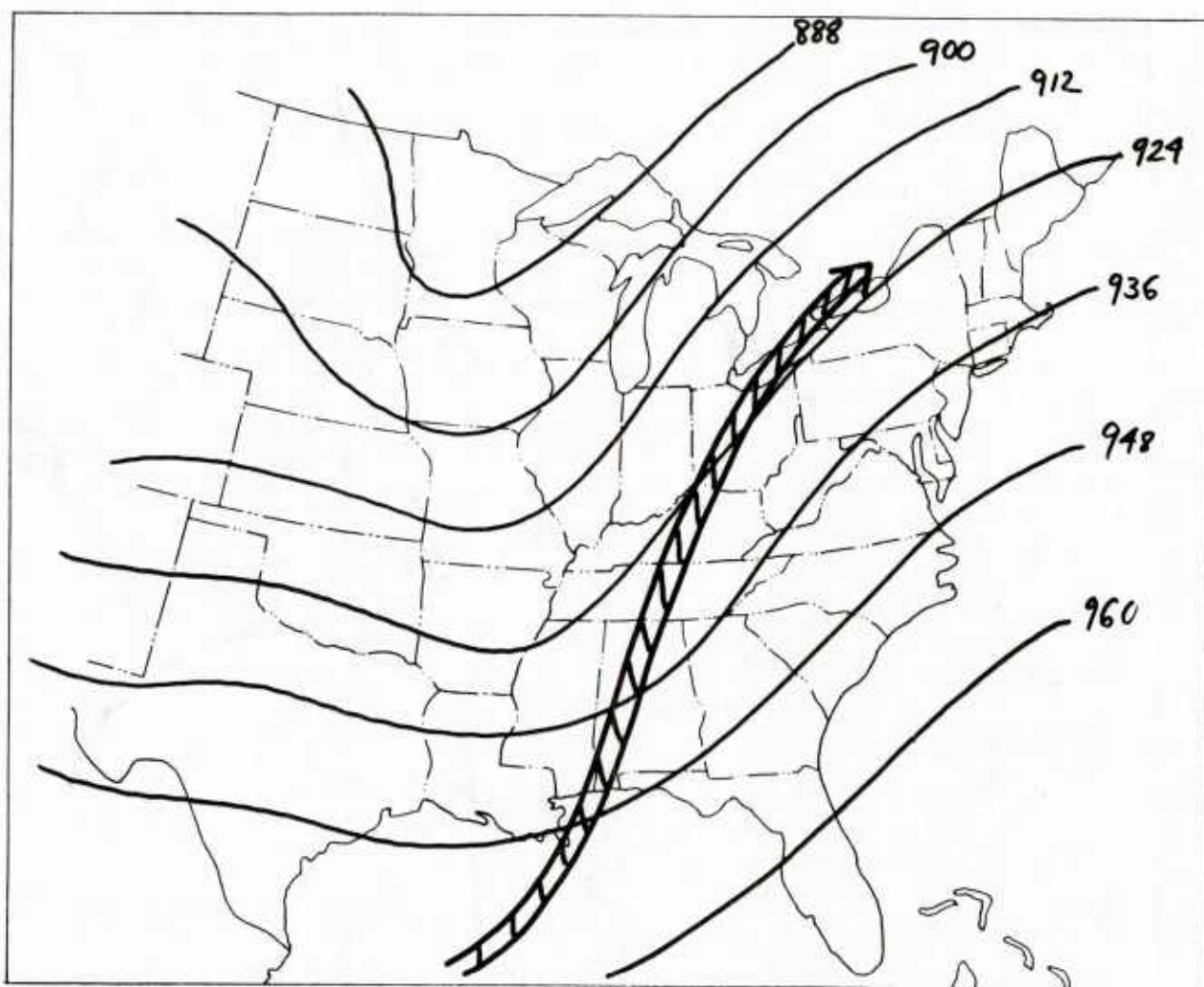
Figure 3.   Elements of the 300 mb chart, 24 Nov 1980, 1200 GMT.

National Meteorological Center's (NMC) analysis, shows a frontolyzing cold front and a surface trough oriented approximately north-south near the left edge of the belt. A surface warm front stretches roughly east-west across the Carolinas with steady rain on both sides. These frontal patterns are characteristic in that fronts are often found in connection with conveyor belts, but they are frequently either diffuse or irregular, and are not always helpful in understanding the rainfall pattern. The belt configuration is usually more helpful in that regard.

Aloft, the jet stream (Fig. 3) lies close to the orientation of the belt and is of the type that is sometimes called a "lifting" jet, with the maximum winds east of the upper air trough. The jet axis crosses the sharp left edge of the cold-topped clouds over southern AL and approaches the right-hand side of the belt over New England. Both of these characteristics--lifting, and crossing at a slight angle--are typical of the cases studied.

On the downstream end, the high-topped clouds generally dissipate somewhat beyond the downstream upper-air ridge. While the right (east) edge is typically rather ragged, the sharp left (west) edge occurs where the warm conveyor belt runs parallel to a dry flow, which may itself be rising in some cases. This sharp boundary has been called the limiting streamline by Carlson (1980) marking the westward limit of air of moist low-level origins. In confluence zones, vertical circulations of the Eliassen type that were first discussed by Namias and Clapp (1949) and explained by Sawyer (1956) and Eliassen (1962) and either modeled or elaborated on by several investigators subsequently, including Bosart (1970), Hoskins (1971) Hoskins et al. (1978), Uccellini and Johnson (1979, and Shapiro (1981), may also be present.

Increasing speeds along the jet axis lead to secondary vertical circulations of the order of a few cm s^{-1}, with upward motion on the anticyclonic

11

side and downward motion on the cyclonic side. Such circulations could play a role in sharpening the edge of the clouds in the middle or upper troposphere. In either event, or if both effects are operating, the sharp left edge is characteristic and is very useful in first identifying, then "navigating" (locating with some precision) the belt.

The dry air to the west of the belt probably came from the rear of the upper level trough where it had subsided, resulting in low relative humidities and low mixing ratios. As it rounds the trough and flows northward parallel to the warm conveyor belt, it can intrude into the moist belt, as Harrold (1973) suggested. This stratification of rising air can lead to release of potential instability. A secondary objective of the present work is to see if there is a favored location relative to the belt for this to occur. Embedded thunderstorms would be favored at such a site.

In sum, the warm conveyor belt is a contiguous region of cold-topped clouds which contains many precipitation-producing elements, sometimes including embedded cumulus convection. Rain, rain fog and low ceilings can be expected over wide regions under the belt.

3. Compositing belts in non-dimensional coordinates.

Based on identification experiments involving several volunteers, it is anticipated that a person using the procedure detailed below who is familiar with the conceptual model of a warm conveyor belt will be able to successfully identify and locate the belt in enhanced infrared satellite imagery in better than three of four cases. The discussion specifically refers to enhanced infrared pictures, based on the common M_B enhancement curve (Fig.4), of the largest cloud structure which meets the following criteria:

COUNT VALUE (INPUT)
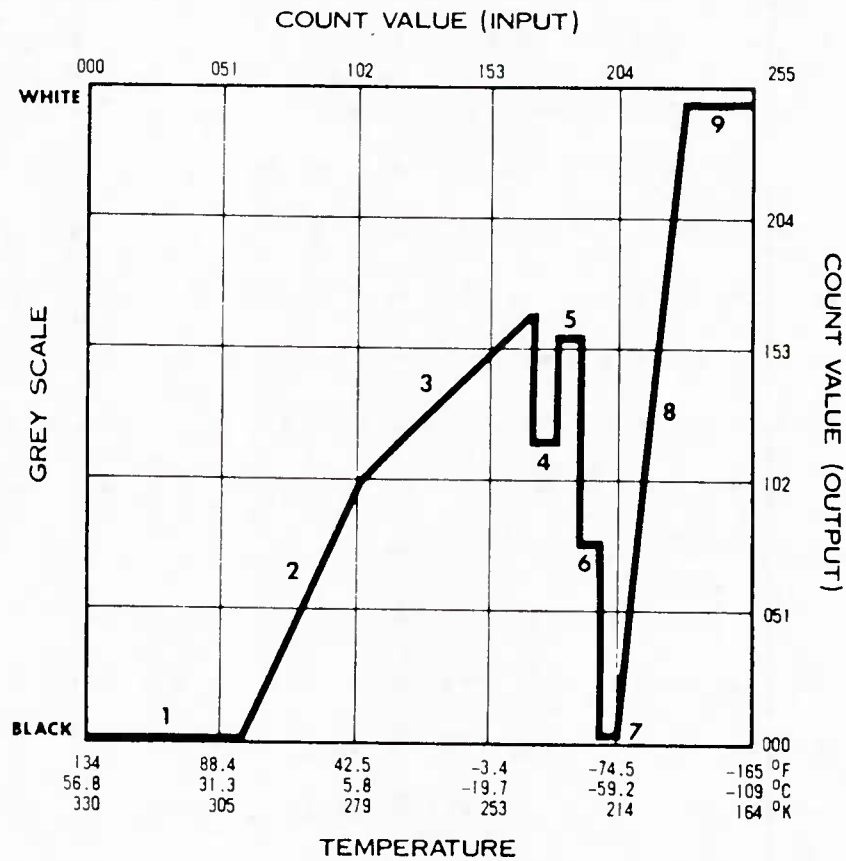
SEGMENT NUMBER	°C TEMPERATURE	COMMENTS	
1	58.8 to 29.3	Little or no useful Met Data (Black)	
2	28.8 to 6.8	Low Level/Sea Surface Difference	
3	6.3 to -31.2	Middle Level - No Enhancement	
4	-32.2 to -42.2	First Level Contour	(Med Gray)
5	-43.2 to -53.2		(Light Gray)
6	-54.2 to -59.2	Thunderstorm	(Dark Gray)
7	-60.2 to -63.2	Enhancement	(Black)
8	-64.2 to -80.2	Overshooting Tops Enhancement	
9	-81.2 to -110.2		(White)

Figure 4.   Enhanced curve M_B for infrared satellite imagery.

1) A conveyor belt possesses a continuous cloud band at least 5 degrees latitude in width at some point along its span, with cloud-top temperatures $\leq -32°C$. The cloud area must be greater than 10 degrees latitude in length. Length is measured along a centerline curve drawn along the direction of the apparent airflow. Width is measured everywhere orthogonally to length. Maximum scales are not pre-scribed, but no cases used had widths greater than about 10 degrees latitude or lengths greater than 27 degrees latitude.

2) The cloud area must have a continuous and well-defined left edge (with respect to a viewer facing downstream). A well-defined left edge has a temperature difference across it of at least $10°C$.

3) The poleward part of the left edge must turn anticyclonically, and the cloud structure must imply a poleward flow component. East-west oriented features are not considered.

After 38 belts which satisfied these criteria were selected, they were composited in a non-dimensional coordinate system based on the centerline of the belt, termed bending coordinates. The bending coordinate system involves a curved central axis (centerline) approximately along the upper level flow, which bends anticyclonically along the belt, bisecting the belt. This is the y-axis. The x-axis is orthogonal to the curving y-axis at every point. The coordinate system, illustrated in Fig. 5 (located in proper position for the belt shown in Fig. 1) is a dimensionless frame of reference fixed to the conveyor belt cloud pattern. The equatorward and poleward ends of the conveyor are assigned $y = 0$ and $y = 2$, respectively. The left edge of the conveyor belt is assigned $x = -1$ and the right edge, $x = 1$, but the range of x is $-2 \leq x \leq 2$, to encompass a substantial amount of the less cloudy air to the sides of the belt. The departure from symmetry permits somewhat greater

14
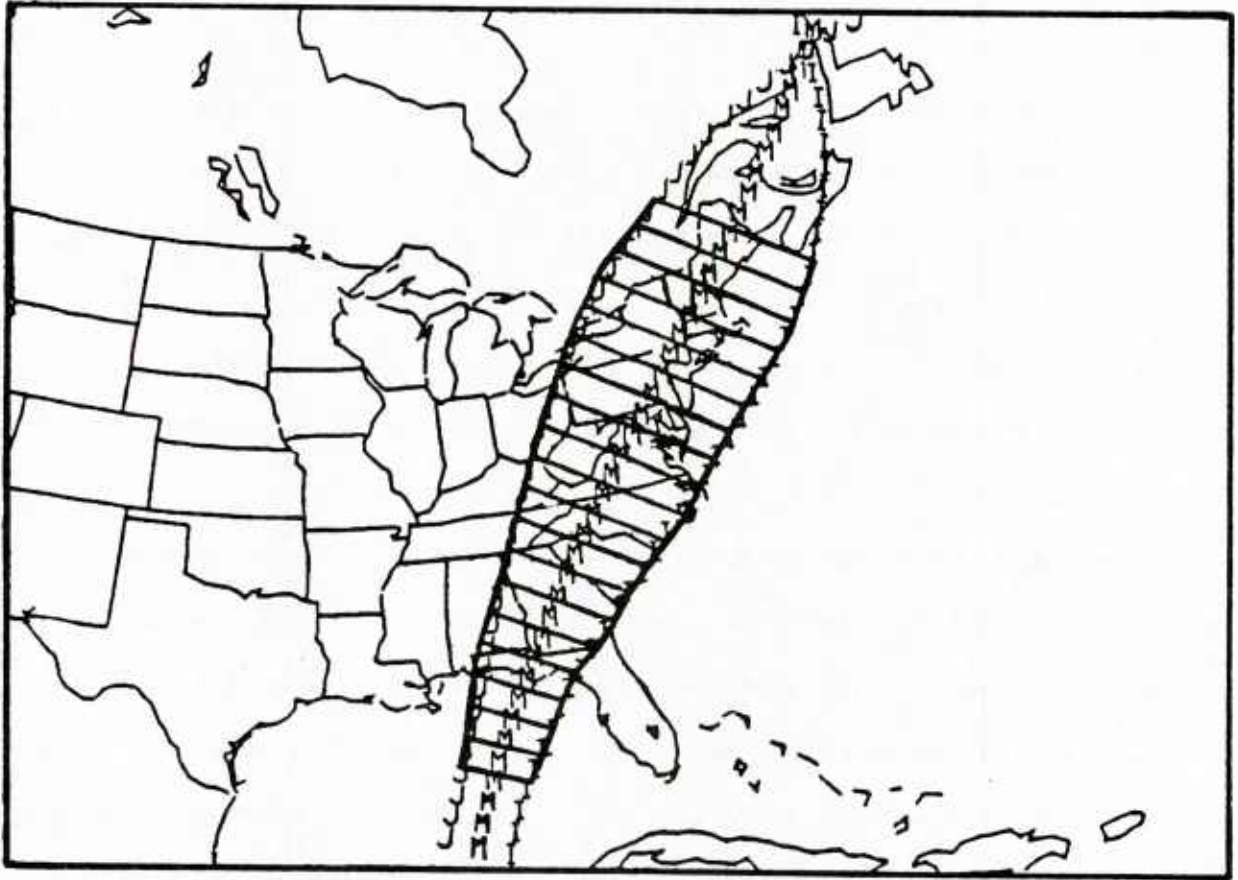
Figure 5.   Example of a conveyor belt (not including adjacent portion of total domain) in which bending coordinate is earth-located.

resolution of the across-stream gradients. Figure 6 shows the bending coordinates expressed in Cartesian form, with the ranges of the coordinate axes. The moist conveyor belt domain is labelled by octants 2,3,6 and 7, with the along-stream halfway point on the centerline in the center of Fig. 6. The non-dimensionalized domain includes four octants (1,4,5,8) in the dry air on each side of the belt.

For the purposes of display, both dimensions were truncated slightly to eliminate some regions of sparse data, boundary distortions, and, in the y-direction, distortions that arise from the narrowing of the conveyor belt, especially at its upstream end. Thus, in Fig. 6, the display ranges are: $-1.8 \leq x \leq +1.8$; $0.2 \leq y \leq 1.8$. As always, $x = 0$ is the centerline, $x = |1|$ is the edge of the belt, and the point $(0,1)$ is the center of the belt in the bending coordinates.

To composite the data, the edges and end points of each conveyor belt were located as follows. The left edge $(x = -1)$ was determined visually from the picture. A rough estimate of the length of the belt was made along the left edge. A first guess of the centerline was then drawn more or less parallel to the left edge. The right edge $(x = 1)$ was located by minimizing the area of clouds with tops warmer than $-32°C$. The right edge is generally more ragged than the left, and thus more prone to subjectivity. This edge is generally a mixture of high cirrus $(< -32°C)$ and warmer middle to high cloud. Some thin cirrus may appear warm due to radiance from lower levels being sensed along with cloud-top radiance. The right edge was drawn roughly parallel to the centerline. The equatorward base (upstream point, $y = 0$) was taken as the upstream point where a break occurs in the left edge of the cloud shield composed of clouds colder than $-32°C$. In other words, the conveyor belt is no longer continuous on its upstream end. The poleward end $(y = 2)$

16
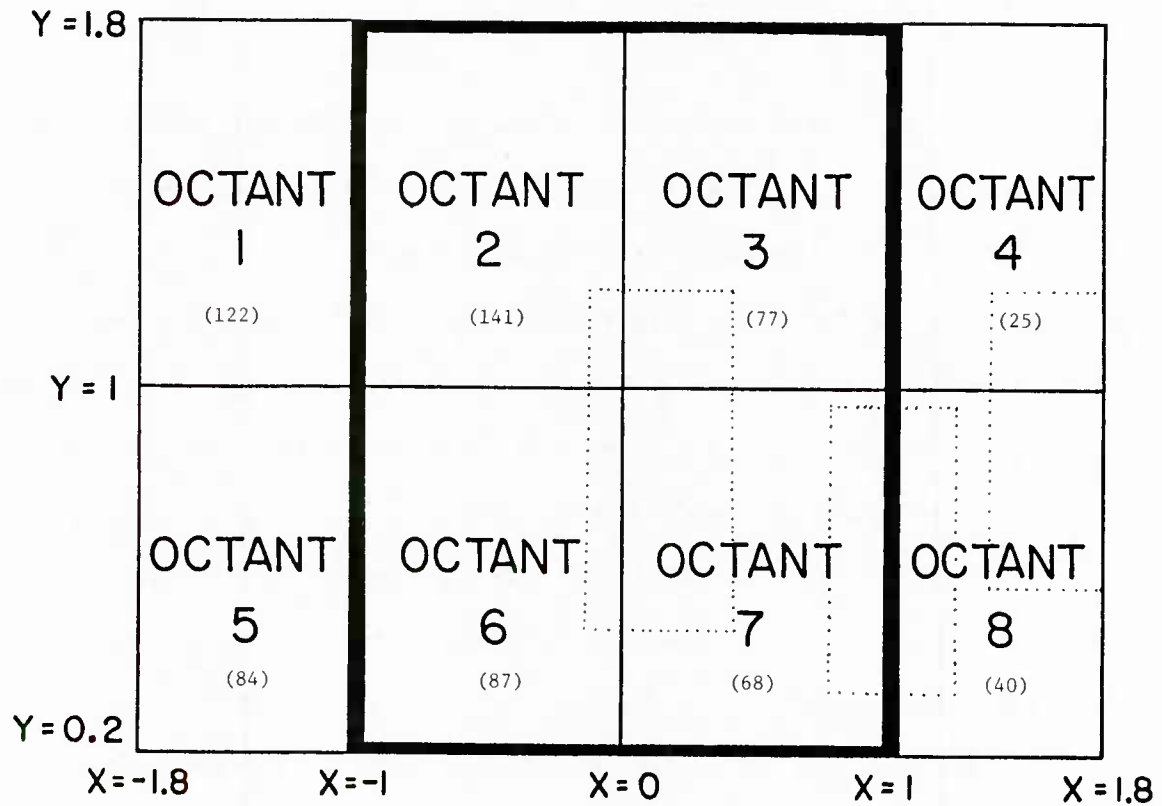
Figure 6.   The bending coordinate domain. Four interior octants comprise
the moist conveyor belt. Domain is truncated slightly at edges.
Also shown are the number of developmental soundings in each
octant and regions (dashed) for test of low level jet.

was located at the downstream point where a break occurred in the cloud shield composed of cloud colder than −32°C. If no break occurred before the left edge turned equatorward, the belt was terminated where it did so, that is, at the apparent ridge line. In a few cases, the belt was terminated where it became narrow. Finally the centerline (x = 0) was finalized by bisecting the two edge lines.

In practice, the belt-location procedure was carried out interactively at a storage-tube computer terminal by moving cross-hairs on a stored map to points viewed by eye on the satellite images and entering those locations (by hitting a key) to identify enough points to encompass the conveyor belt. A program then automatically fitted two curves to these points using third order polynomials, calculated the centerline, and converted screen coordinates to bending non-dimensionalized coordinates.

After a belt was navigated (earth-located), each data point (radiosonde observation) from a particular case was composited in terms of its fractional distance to the boundaries of the domain.

Thirty-eight conveyor belts were selected from the 1978-1981 period. These 38 cases produced 644 soundings taken within 3.5 hours of the satellite picture from which the belt was selected. These developmental cases are listed in Table 1. The conveyor belts varied in size, orientation, and geographic location, but do have similar shapes. That is the way they are recognized. All of the belts occurred over the eastern United States, generally near the Atlantic Coast.

The distribution of data in the developmental sample was not uniform. The number of developmental radiosonde observations in each octant are shown in parentheses on Fig. 6. A domain placed over the eastern United States suffers when conveyor belts approach the coast, in that there are few sondes

18

TABLE 1. Observation times of soundings from the 38 cases of the
          developmental sample for conveyor belt composites (0000
          GMT 09JA78 is 0000 GMT, January 9, 1978).

Developmental Sample

0000 GMT 15DE77	1200 GMT 21JA79	1200 GMT 14NO80
0000 GMT 09JA78	1200 GMT 24FE79	1200 GMT 23NO80
1200 GMT 09JA78	0000 GMT 25FE79	0000 GMT 24NO80
1200 GMT 12JA78	0000 GMT 24NO79	1200 GMT 24NO80
0000 GMT 13JA78	1200 GMT 24NO79	1200 GMT 08DE80
1200 GMT 17JA78	1200 GMT 25NO79	1200 GMT 09DE80
1200 GMT 07JA79	1200 GMT 04JA80	1200 GMT 10DE80
0000 GMT 08JA79	0000 GMT 05JA80	0000 GMT 10FE81
1200 GMT 08JA79	0000 GMT 02MR80	1200 GMT 10FE81
1200 GMT 12JA79	1200 GMT 18MR80	0000 GMT 11FE81
0000 GMT 19JA79	1200 GMT 12AP80	1200 GMT 11FE81
1200 GMT 20JA79	0000 GMT 18OC80	1200 GMT 19MY81
0000 GMT 21JA79	0000 GMT 24OC80	

available on the east flank, especially in the dry air of octants 4 and 8. Only about 10 percent of the radiosondes were taken in that quarter of the domain. Accordingly, conclusions concerning that dry flank are sketchy, at best.

Compositing was performed in the non-dimensional bending frame of reference by a successive corrections objective analysis. All analyses were performed on a 30 x 40 grid giving an approximate resolution of 50 km along and 25 km across the conveyor belt. First, initial values were obtained at the grid points whereby all observations within a radius of 8 grid points were weighted equally. This practice contributes to a smooth field in data-sparse regions of the grid. Second, this field was smoothed using three passes of a 1:4:1 smoother. Third, the grid points were corrected on the basis of the successive corrections method using a radius of 4 grid points. Fourth and finally, this field was smoothed with three passes of a 1:4:1 smoother. This approach was selected as the best of a number of methods tested, preserving some conveyor belt substructure, and minimizing noise contributed from individual data points.

Direct smoothing and the smoothing implicit in the successive corrections analysis serves to reduce case-to-case variation. Unlike meteorological fields obtained from simultaneous data, in which the scale of features resolved is limited by the data density, composite fields have rather dense data coverage, but much noise introduced by differences between cases. Smoothing is necessary, but the optimum technique is not known a priori because from the developmental sample it is impossible to determine the scale of meteorological signal present. Accordingly, some subjective meteorological judgement was invoked in analysis and smoothing.

Developmental composite analyses were performed for the wind components and for the wind direction and speed as well as the relative humidity. Temperature was not done because seasonal temperature variations would introduce much noise. For purposes of numerical weather prediction, a consistent temperature field could be recovered from the winds. Radiosonde observations preserve vertical detail, but much case-to-case noise is involved in the vertical, as well as the horizontal. Accordingly, the composite conveyor belt will be presented in "3-layer model" form, to depict the region near the top of the boundary layer, the mid-tropospheric levels of upward motion, and the cloud-top levels near the jet stream that are most easily recognized in satellite imagery. As a vertical consistency check, analyses were performed at fifteen levels separated by 50 mb, but the discussion and figures will concentrate on the 950, 650, and 350 mb levels in most respects.

4. Humidity and wind composites of the warm conveyor belt at 350, 650, and 950 mb.

Figures 7, 9 and 11 depict the composite structure of relative humidity (with respect to water) and wind direction and speed at 350, 650 and 950 mb respectively. Relative humidity is presented both as a matter of interest and also to help the reader relate the wind flow to the cloud patterns. In Fig. 7a, the relative humidity with respect to water at 350 mb shows a quite uniform field of high humidity in octants 2,3,6, and 7, with rather large gradients near the octant boundaries. Allowing for the ice/water difference in saturation vapor pressure, this figure presents essentially what one would expect from the satellite images, with rather uniform cirriform clouds bounded by dry air. The upstream (equatorward) origin of the belt suggests a somewhat different picture, with somewhat more dry air within the (usually narrower)

21
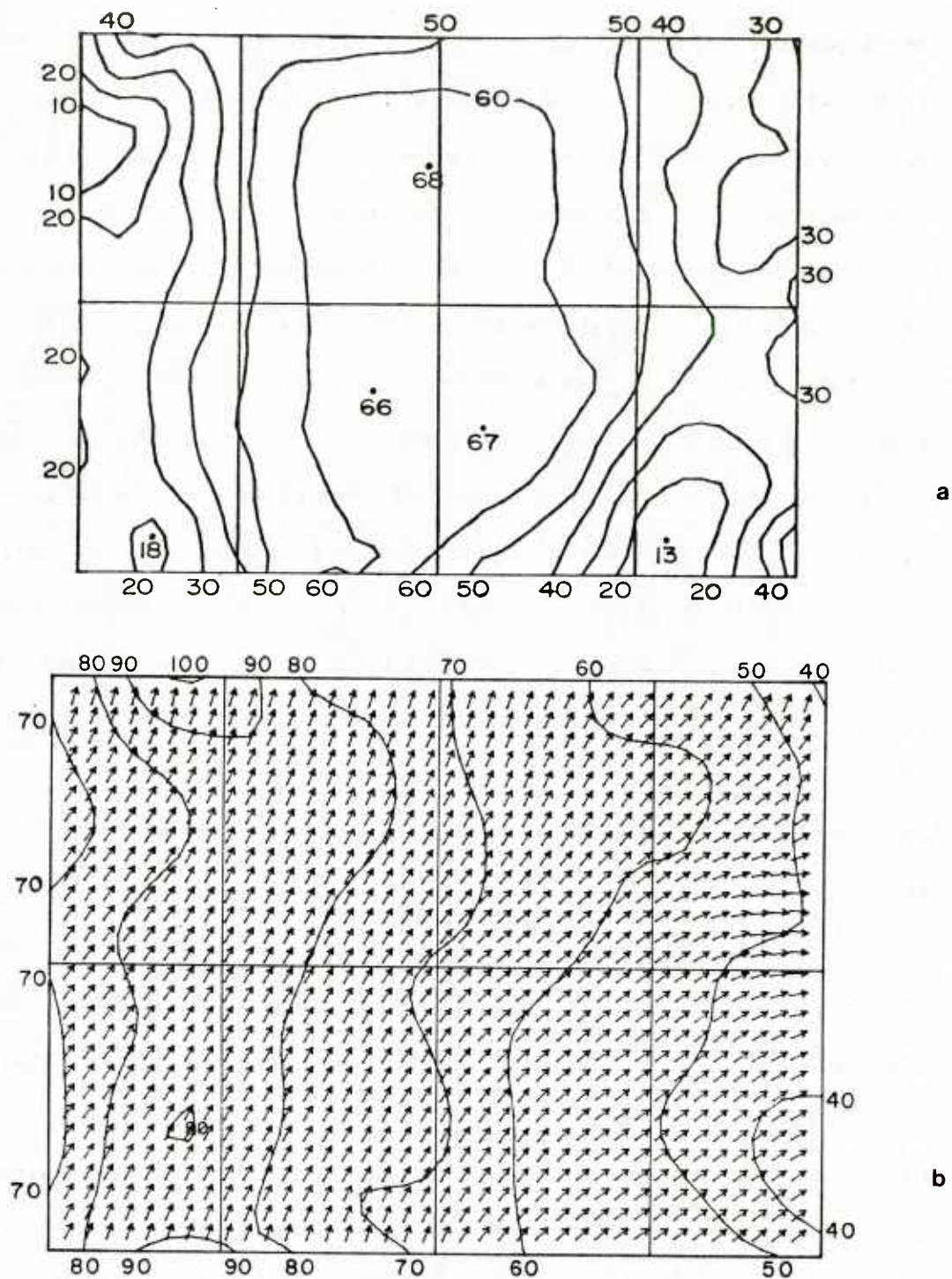
Figure 7.   Composite structure at 350 mb of (A) relative humidity (percent)
and (b) wind directions (arrows; upward on page implies
parallel to centerline of belt from equatorward end to pole-
ward end) and speed (kt), from developmental sample.

beginnings of the belt. This is probably related to the belt originating in lower regions of the atmosphere and the cirriform part here being pumped up by smaller-scale convection of less uniform nature.

The associated wind pattern is shown on Fig. 7b. Arrows represent the wind direction at the model grid points and isotachs display the speed. These are not relative winds; instantaneous system phase speed is difficult to determine and may vary across the belt. They are, however, displayed in the bending coordinates, so that they are no longer west and south components on an earth-located coordinate system.

However, for interpretation purposes, it is useful to display the winds with respect to the sharp left edge of the belt. To accomplish this, each reported radiosonde wind direction was reoriented by an angle equal to the departure of the angle of the nearby centerline of the belt from the meridians. The local value for each radiosonde report was determined by projecting a perpendicular from the centerline of the belt through each radiosonde report. The resulting angular correction angle (α) is illustrated on Fig. 8. Reoriented wind components were then analyzed to generate the wind directions displayed on Figs. 7, 9, and 11. The practical effect is to display wind directions as though the left edge were a straight line extending up and down the page. A wind cutting across the x = -1.0 line at a $\pi/6$ angle cuts across the (left edge of the) belt at the $\pi/6$ angle, whatever the orientation of the belt. These winds are reoriented to display instantaneous flows (at the time stage when the cloud belt is well developed and anticyclonic, but not part of an intense cyclone) with respect to an arbitrarily oriented conveyor belt involving poleward flow. They are not relative winds, however.

23
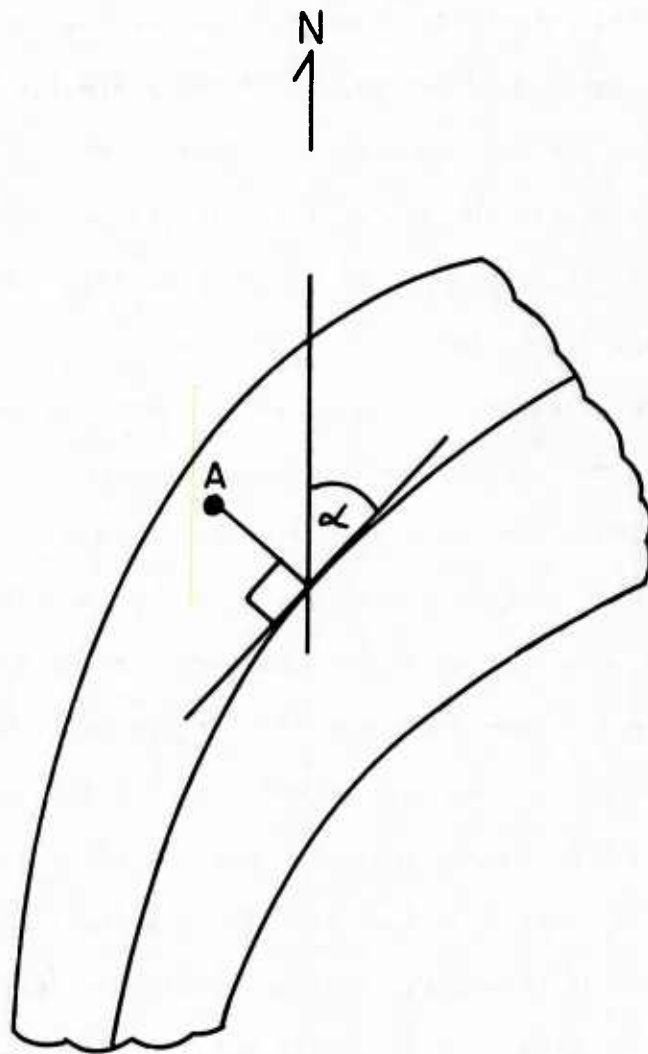
Figure 8.   Illustration of reorientation (through α) of reported
             winds with respect to centerline prior to analysis.
             Rawinsonde wind report at Point A is rotated counter-
             clockwise by α prior to analysis to depict winds as
             though centerline was oriented straight north-south.

24

Figure 7b shows that the upper level winds are somewhat difluent across the belt in the composite. As a steering flow, these winds should "lift" the belt poleward and somewhat to its right. Weakening short-wave troughs accelerating poleward on the Northern Hemisphere are sometimes referred to as lifting troughs. While there is no information in these composites about the composite wind speeds on the west side of the 350 mb trough, the high composite speeds depicted on Fig. 7b (80-90 kt) is consistent with maximum winds on the east side of the trough, the pattern that is associated with lifting.

The jet stream axis lies close to the sharp left edge of the cirrus shield at 350 mb, but crosses it at a slight angle, entering somewhere near y=1, the halfway point in the along-belt direction. A second jet occurs along the left edge far downstream. The crossing angle is about 25 degrees at that point. Taking a rightward phase speed of about 25 kt, derived from the bending coordinate reoriented u-component at 650 mb near the middle of the belt, the _relative_ wind direction in reoriented bending coordinates lies along the left edge and comes to within 6 degrees of being parallel to the belt. This lends good support to Carlson's (1980) interpretation that the relative wind blows parallel to the left edge of the belt with the edge being the limiting streamline of air from moist sources.

An alternative explanation of the sharp left edge, a vertical circulation of the Sawyer-Eliassen type, could be invoked if the jet stream winds were confluent, speeds increasing downstream. Such circulations undoubtedly play a role in many conveyor belt systems, but the case for them in the composites is not strong. Except for the downstream jet noted above, the speeds are quite uniform along most of the left edge and the overall pattern of directions is weakly difluent. Thus, confluence is probably only a small factor in

25

sharpening the left edge. Taking v as the along-belt component and assuming the smooth winds are geostrophic in the y-direction, $v_g \frac{\partial u}{\partial y}$ is small everywhere except at the downstream end of the left edge. Shearing advection may play a role in sharpening the left edge at the octant 5/6 boundary, consistent with evidence of cross-belt flow toward cold air in the mid-belt region.

In any event, the jet stream lies close to the sharp left edge, and anticyclonic horizontal shear prevails over the bulk of the cold-topped cloud and precipitation region, implying that conditions for symmetric instability (Emanuel, 1979) may well be found within the belt.

At 650 mb (Fig. 9a), the relative humidity and implied cloud pattern begins to depart from the rather simple picture suggested by the cirriform tops of the belt. While there are still strong humidity gradients on each side of the belt, there is a distinct bulging of moist air into the dry regions to the left of the belt just downstream of the alongbelt center (y = 1). This bulging is part of a humidity maximum that occurs in octant 2 left of the centerline. It is similar to the slight bulging of clouds into cold air that signals cyclogenesis along a cold front cloud band. A secondary maximum also occurs left of the centerline near the upstream source, part of the narrow humidity maximum found in that region at 350 mb, also. In fact, the left half of the belt (octants 2 and 6) appears on the whole to be somewhat more humid than the right side, although the mean difference is only 11 percent, 77 versus 66 percent.

With respect to winds at 650 mb (Fig. 9b), the streamline pattern is similar to that at 350 mb, with some veering of wind direction upward in the right hand octants 3,4,7 and 8, and some backing upward in the left-hand octants 1, 5 and 6. There appears to be little upper level temperature advection in octant 2. This temperature advection pattern along with dry

26

advection at 650 mb in octant 6 is very consistent with destabilization occurring in the cloudy air of this quadrant. It should be a favored region for embedded convection.

Furthermore, components along the belt predominate over components across the belt in these precipitation-producing levels, with a very uniform fast, along-belt flow characterizing the cloudy air. Unlike above (and below) horizontal shears are rather weak in middle levels. The conveyor belt flow can be seen more clearly, however, when the along-belt component (only) at 650 mb is shown (Fig. 10). Positive (blowing along-belt) and rather uniform speeds of 30-40 knots prevail within the belt. Along-belt speeds drop off in the air on either side of the conveyor belt. The picture that emerges is that of a fast-flowing moist current of approximately the same width as the cold-topped clouds above it, with tangential shears in the along-belt component near the edges of the belt.

Also, the flow to the left of the belt has a positive along-belt component. Even after allowance is made for the turning of the belt itself, it appears that the cold air has little or no northerly component in earth-fixed coordinates. With normal cold front slopes of 1:100 or so, such components would be expected. Instead, there are weak or absent northerly flows in the cold air, consistent with the sort of flow often found behind lifting troughs, where strong cold air driving equatorward is unusual.

In the region from which the sample radiosondes were drawn, station pressures are typically 960-1020 mb. Accordingly, 950 mb observations (Fig. 11) are either within the boundary layer or slightly above it. The relative humidity at this level (Fig. 11a) is very different from what is found higher in the conveyor belt. Here, the humidity is more uniformly high, both under the belt and outside it, although a weak maximum does occur in octant 6,

28
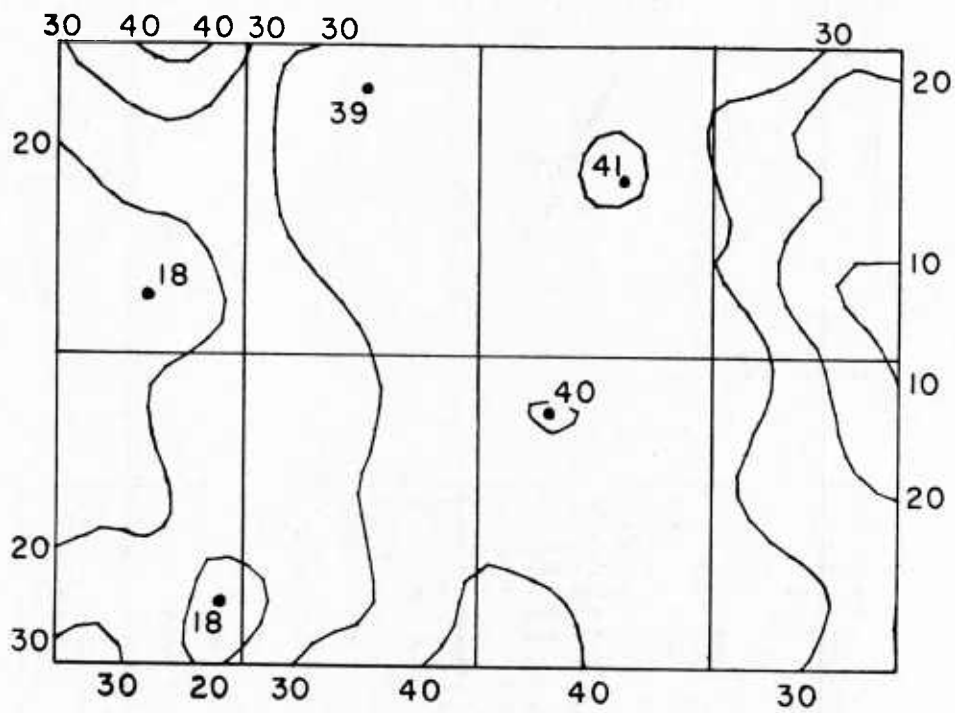
Figure 10.   Alongbelt (v) component (kt) at 650 mb, developmental cases
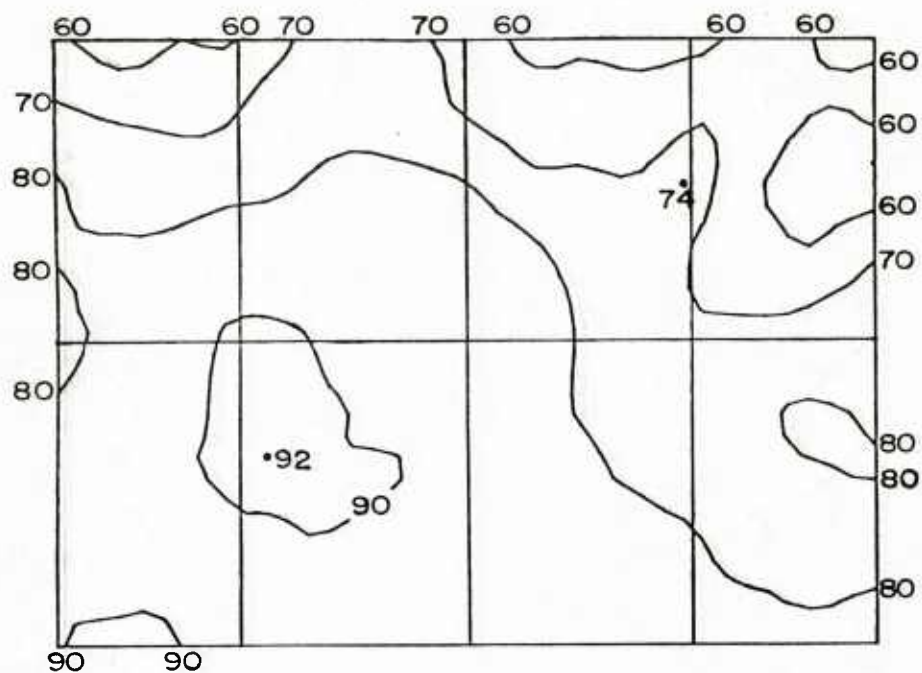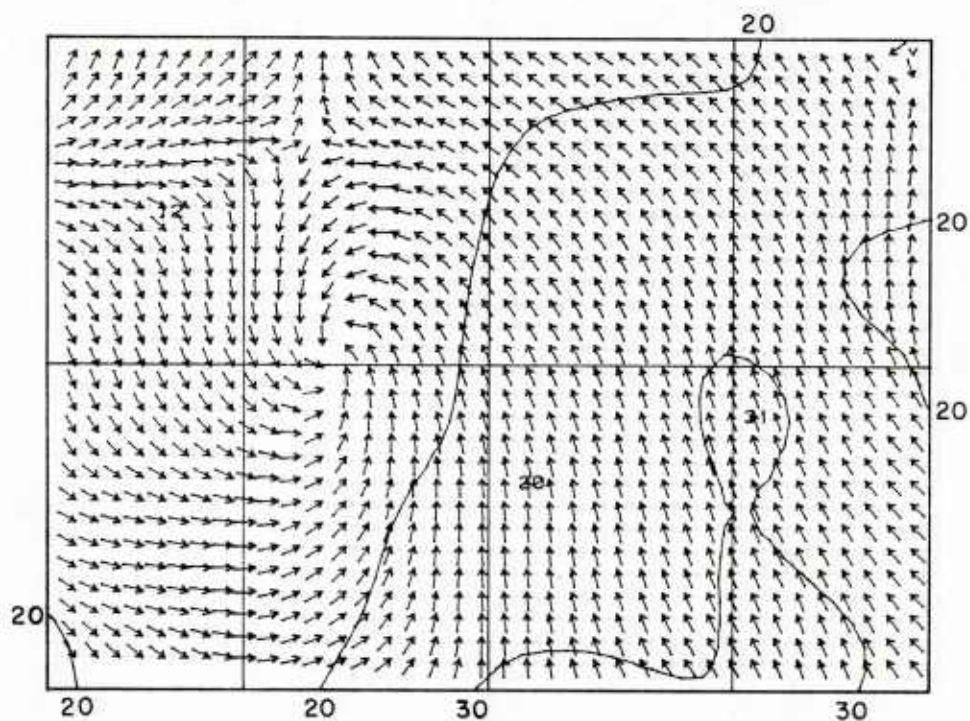
Figure 11.   As in Fig. 7, at 950 mb.

possibly as a consequence of previous precipitation into this layer. Generally, humidities decrease somewhat more in the along-belt direction than across the flanks and the low-level field shows less conveyor belt-related disturbance than higher levels do.

The low-level winds, however, display many interesting features. A striking cyclonic circulation appears, centered a very short distance in the along-belt direction beyond the octant 2-octant 6 boundary (just beyond $y = 1$) about midway between the centerline and the left edge of the conveyor belt. Although no effort was made or intended to locate cyclones in relation to conveyor belts (indeed, well developed cyclones were excluded), the composites suggest that successful identification of a conveyor belt in satellite imagery in data-poor regions, such as over oceans, might permit one to estimate the most probable location of a weak or developing cyclone. One would locate the belt and its centerline and estimate a wave position halfway to the left edge from the centerline at $y \cong 1.1$.

From the streamlines, it can be seen that in the right hand octants, plus octant 2, the wind veers substantially between 950 and 650 mb, again emphasizing the role of warm advection in conveyor belts. True conveyors should not occur in the classical barotropic warm sector. To the left of the belt there is cold advection, and in octant 6 a line of demarcation between cold and warm advection consistent with a cold front location under the belt of clouds halfway from the centerline to the left edge. This front position would be appropriate for a wave located at $(-0.25, 1.10)$ as discussed above.

Of special interest is the low level wind maximum which lies along the right flank of the belt almost precisely under the edge of the high clouds (octant 7-8 boundary). This feature, which reaches 28 kt in the v (along-belt) component in the developmental set and 34 kt in the independent test sample, is

31

very intriguing in terms of the sharpness of the right hand flank and in terms of the dynamics of the belt itself. In connection with this low-level wind maximum at 950 mb, a very large relative vorticity gradient is found on the right flank in the inflow region. Ekman pumping of air that is already disposed to upglide may play a role in the octant 7 cloudiness and precipitation, with a sharp cut-off at a low-level jet.

Hence, on the right-hand upstream flank (octant 7/8 boundary), there is a potential location for bogussing a wind maximum along the cloudiness edge. Alternatively, prediction models that forecast winds well might be interpreted to place the right-hand flank of these belts, a difficult task heretofore.

Figure 12 shows the 950 mb relative vorticity from the developmental sample. There is a preference for positive values under the belt, and negative values outside it, but there are exceptions. Maximum vorticity lies along the frontal zone in octant 6, and also arcs from the vicinity of the cyclonic circulation under the left side of the belt through octants 2 and 3 and equatorward through octant 7 along the cyclonic side of the low level jet. This secondary vorticity maximum near the right flank of the belt bears some relationship to the feature modeled by Hoskins and West (1979) for a channel flow with uniform potential vorticity and a jet stream in the channel, which the authors called warm front type A. In their results, this feature is an outcome of specifying a jet stream aloft, rather than a uniform current. This is suggestive that the alongbelt fast flow at 700 mb is coupled to the low level jet dynamically. However, the horizontal scale of the feature under discussion is considerably smaller than the low order modes modeled by Hoskins and West.

In any event, the octant 7 region of this front-like feature is much more moist than octant 8 in the middle troposphere. At 650 mb, the median relative

32

Figure 12.   Relative vorticity (x $10^{-5}s^{-1}$) at 950 mb, developmental sample.
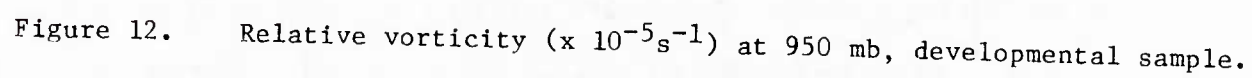
humidity observation in octant 7 is 83 percent in the developmental sample (61 observations) in contrast to 15 percent in octant 8 (37 observations).

Thus, the developmental sample presents a low-level pattern of a hidden cyclonic circulation under the cloud belt, with its associated fronts, low level jet, and moisture fields. In midtroposphere, a fast uniform flow with flanking shears and high humidities (highest in octant 2) flows rapidly poleward. At this point it is appropriate to consider the extent to which these features are sample-dependent.

5. Comparisons with an independent sample

a. Wind comparisons

Twenty-three additional conveyor belts were identified from the 1981-83 period. The same compositing and analysis procedures were applied to these cases as were done in the developmental sample. This generated two 30 x 40 arrays, which are compared in Tables 2 and 3.

In Table 2, means and standard deviations for the samples are tabulated for each of the 3 levels. Generally, the belts in the test sample were drawn from cases exhibiting stronger winds, with speeds averaging 1.4, 5.1 and 13.1 kt greater at the 950, 650 and 350 mb levels, respectively. Standard deviations of speed were larger, as well. The same held true for the alongbelt and acrossbelt components (not tabulated); component magnitudes and standard deviations were larger in the test sample.

In keeping with stronger wind speeds, relative vorticity values showed larger standard deviations in the test cases except at 350 mb where they were smaller. Also, the mean vorticity was more cyclonic in the low-levels, again consistent with somewhat stronger systems involved in the test cases.

34

TABLE 2. Comparisons between Developmental and Test Samples

FIELD	LEVEL					
	950 mb		650 mb		350 mb	
	Mean	Standard Deviation	Mean	Standard Deviation	Mean	Standard Deviation
Wind Direction (deg)						
Developmental	176.	37.	213.	12.	214.	11.
Test	155.	40.	212.	11.	215.	13.
Wind Speed (kt)						
Developmental	20.8	5.9	39.1	5.7	68.2	13.7
Test	22.2	6.4	44.2	10.1	81.3	15.2
Relative Vorticity $(\times 10^{-5} \text{ s}^{-1})$						
Developmental	0.6	2.1	0.4	2.3	$-$ 0.9	4.2
Test	1.3	2.3	0.7	2.6	$-$ 1.27	3.4
Relative Humidity (%)						
Developmental	80.	21.	61.	36.	50.	27.
Test	83.	18.	64.	35.	51.	16.

In that connection, the mean wind direction at 950 mb was 15 degrees further in the direction of inflow from the right flank, also consistent with more vigorous systems. Aloft, the mean vorticity was more cyclonic in the low levels, again consistent with somewhat stronger systems involved in the test cases. However, the directions aloft were highly correlated in the two samples.

Overall, the test sample cases appear to have systematically involved more vigorous cyclonic features. Whether an excess of zeal to add test cases operated to produce this bias is hard to judge, but some of the comparisons between the samples suffer as a result of it.

Table 3 displays some linear correlation coefficients for the two samples. These were arrived at by pooling grid point values in each sample. The numbers of grid points overstate the information available in the developmental composite. Correlations based on an estimate of the number of independent pieces of information that might be extracted would be preferable, but these inter-correlations give a rough measure of the validity of the composites when applied to new cases.

The correlations for the entire 1200 grid point ensemble, including the belt and the dry adjacent regions, are labelled ALL; points within the central portion of the moist belt, truncated at $x = -1.0$ to 1.0, and $y = 0.5$ to 1.5, are labelled BELT. This is the region of greatest interst, in the vicinity of the cyclonic circulation and high humidities.

The wind field correlations tend to be best aloft and weaken downward. A notable exception occurs in the 650 mb wind speed, where for the full belt, the 650 mb correlation drops off to 0.38. This appears to be related to lower correlation in the alongbelt component (not shown). Otherwise, speed

36

TABLE 3. Correlations between Developmental and Test Sets

FIELD	LEVEL					
	350 mb		650 mb		950 mb	
	ALL	BELT	ALL	BELT	ALL	BELT
Speed	.89	.89	.38	.58	.65	.65
Direction	.72	.79	.62	.69	.45	.45
Vorticity	.63	.67	.49	.78	.46	.46

correlations are somewhat better than direction at all levels, indicating some change in wind pattern.

The vorticity correlations are consistent, being larger aloft than at 950 mb. Figure 13, which depicts the 950 mb winds in the test sample, shows that the cyclonic wind field in the test sample has important differences. The winds are more suggestive of a well-developed cyclone external to the belt, with some type of occluded front reaching in under the belt. Indeed, all indicators point to more development in the test sample, and there is some question whether analysts can consistently differentiate well-developed cases from the nascent or weak waves that were imputed in the study. About all that can be said is that the location of the maximum low level vorticity is similar in both samples, suggesting that a feature can be expected there, apparently traveling with the belt. However, the nature of the disturbance must be taken as being unknown.

The association between the right-hand edge of the belt (octant 7/octant 8 boundary) with the low-level wind maximum was checked by use of a Mann-Whitney test of the difference in median reported wind observations at 950 mb in the regions indicated with fine dashed lines on Fig. 6. The low-level jet region straddles the octant 7-8 boundary, and its speed observations were compared to the regions shown, where speed minima existed in the developmental sample.

Table 4 gives the relevant data for the comparison. The speed at the maximum is somewhat weaker in the test sample, and the shear is notably weaker. The generally stronger winds of the test sample may be contributing to this. In both cases the number of observations is small, this region sometimes being in the data-void area off the coast. With respect to the developmental set, median speeds in the jet are stronger than those on either flank at the 99.9% confidence level, but the weaker shears and smaller number of observations

38
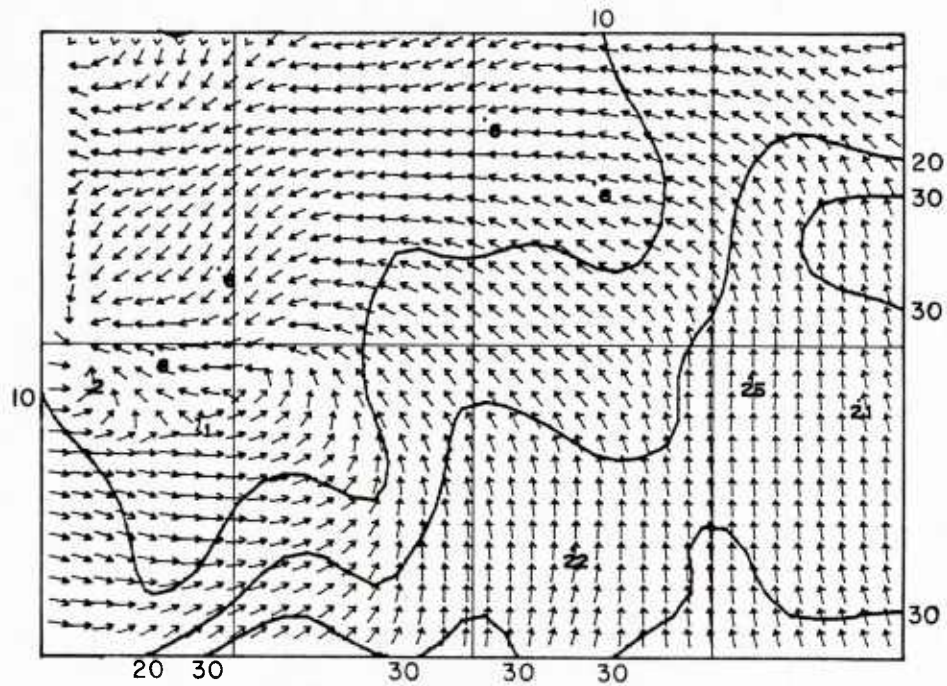
Figure 13.   950 mb wind direction and speed, 23 independent cases. Data
presented as in Fig. 11b, for comparison.

TABLE 4. Comparison of Wind Observations in Region of Low-Level Jet
with Adjacent Areas (See Fig. 6 for Boundaries)

Wind Speed (kt)	Left Flank		Low-Level Jet		Right Flank	
	Dev. Set	Test Set	Dev. Set	Test Set	Dev. Set	Test Set
Observations	43.	17.	17.	7.	17.	11.
Mean	13.3	21.0	30.7	27.9	9.2	22.5
St. Dev.	18.0	16.0	15.7	16.9	15.1	9.4
Median	10.0	21.0	31.0	25.0	8.0	19.0

reduce that confidence to 81% (to the left) and 84% (to the right) in the test sample. The strength and consistency of this low-level wind maximum needs to be evaluated further, but there is probably sufficient reason to believe that it exists, at least for belts over eastern North America.

b. Moisture comparisons

An independent test of the developmental humidity model was conducted on a smaller test sample comprised of 11 cases. The independent set, consisting of 130 radiosonde observations, served as the verification values (VERIFICATION). Calculations were made of the root-mean-square errors between the VERIFICATION file and the composite humidity model (MODRH) as well as four separate estimates of relative humidity. The four fields used were: (1) the sample mean, (2) climatology, (3) a random uniform distribution and (4) the Forecast Output User Statistics (FOUS) 12-hour forecasts of 700-500mb and boundary layer humidity. The rms errors of these four fields were then compared to the rms errors of the developmental humidity model in order to measure the performance of the model.

The FOUS data is part of the output of the limited-fine-mesh (LFM-II) model run by the National Meteorological Center (NMC). The prediction is a 12-hour forecast verifying at the synoptic time (0000 and 1200 GMT) of the VERIFICATION file test case. The sample mean, a horizontally constant field of relative humidity, is the mean of the independent data. Another horizontally smooth field, climatology, was calculated using January relative humidity values at 30°N and 45°N latitude taken from the United States Standard Atmosphere. The random uniform distribution uses a random number generator to select values uniformly distributed on the integers over a specified interval. At 650 mb, values between 5 and 100% were used. Five percent was chosen as the

41

lower limit, as relative humidities below that are uncommon in the atmosphere. At 950 mb, values between 50 and 100% were used.

Individual relative humidity values for each field were compared at the coordinates of the VERIFICATION data points. The coordinates of the observation sites were specified in two ways: (1) the latitude and longitude taken from a polar stereographic projection, and (2) the bending x-coordinate and y-coordinate taken from the non-dimensionalized system. The FOUS values are not always at collocated VERIFICATION coordinates and therefore were analyzed onto a 30 by 40 grid in order to interpolate relative humidity values to the location of each upper-air station.

Before interpolating, the FOUS data was fitted to the 30 by 40 grid using a method of successive corrections and smoothed using one pass of a 1:4:1 smoother. The MODRH files are also 30 by 40 gridded analyses, but in bending coordinates. As with the FOUS data, an interpolation scheme was used to obtain relative humidity estimates from the model at coordinates identical to those of the upper-air stations. These humidity estimates were calculated for both the 650 and 950 mb levels.

A comparison of the rms errors between the developmental model and both the dependent and independent data sets reveals very little difference. For all eight octants the rms error of the 566 data points in the dependent sample was 30.2% compared to 32.5% for the 110 observations in the independent sample. Table 5 lists the rms errors for all five fields along with standard deviations and means for each population. The MODRH data set exhibited a smaller rms error than three of the four fields tested, with only the FOUS data set scoring lower. The absolute differences between MODRH and the sample climatological mean, the random normal distribution and climatology were large, on the order

42

Table 5. Statistics for all eight octants of the independent data set at the 650 mb level. The data fields consist of radiosonde observations (VERIF) and interpolated predicted values from the developmental relative humidity model (MODRH) and the LFM-II (FOUS). Parenthetical values are sample size; bracketed values are relative humidities of the horizontally flat fields.

Fields	Rms Error (%)	
VERIFICATION vs. MODRH	32.45	(110)
VERIFICATION vs. FOUS	31.54	(110)
VERIFICATION vs. SAMPLE CLIMATOLOGY MEAN	35.3	(59.6%)
VERIFICATION vs. CLIMATOLOGY	37.3	(46%)
VERIFICATION vs. RANDOM UNIFORM DISTRIBUTION	42.4	---

Fields	Mean (%)	Standard Deviation (%)
VERIF	59.62	34.4
MODRH	60.06	19.0
FOUS	73.97	26.4
VERIF – MODRH	– 0.44	32.8
VERIF – FOUS	–14.35	28.4

43

of 3 to 5%[*], while the absolute difference between MODRH and FOUS was only 0.9%.

Some interesting figures in Table 5 are the mean and standard deviations of the independent data set, the 12-hour FOUS forecast and the developmental model. It appears that the FOUS data set has a moist bias, as is shown by the mean of the difference between the VERIFICATION and FOUS observations, -14.35%. The means of the VERIFICATION and MODRH data sets are almost identical. However, when the latter two data sets are compared, a large rms error is evident. A possible explanation may be found in the standard deviations of the two samples. Examining the standard deviations indicates a substantial difference in the range of observations for the VERIFICATION (34.4%) versus MODRH (19.0%) samples. The low variability of the model represents efforts to alleviate the small-scale noise inherent in compositing. The smoothing and averaging schemes employed effectively smooth out the low and high ends of the frequency distribution.

Although synoptic-scale structure of the conveyor velt and surrounding environment is adequately reproduced by the model, maxima, minima and humidity gradients have been diminished. This can lead to large rms errors in regions where humidity variations are large. A good example of this is in octant 5. Table 6 is an octant-by-octant description of rms errors showing a large rms error for MODRH in octant 5. A hand analysis of the data reveals a bimodal distribution with 50% of the points being extremely dry ($\leq$ 30%) and 33% being greater than 80%. The minimum value observed in the model's 650 mb analysis

---

[*] This is an absolute difference between two percent values, as opposed to a "percent difference" which divides the absolute difference by a reference value.

44

Table 6. A statistical description of the eleven case independent data set at the 650 mb level. The data fields for each of the eight octants comprising the model domain are identical to those of Figure 5. N is the sample size.

Octant 1

Fields	Rms Error	N
Verif-Modrh	34.59	18
Verif-Fous	28.03	18

Fields	Mean	Stan. Dev.
Verif	62.1	29.7
Modrh	51.3	8.0
Fous	76.7	21.9

Octant 2

Fields	Rms Error	N
Verif-Modrh	22.06	21
Verif-Fous	23.43	21

Fields	Mean	Stan. Dev.
Verif	78.4	25.4
Modrh	82.0	10.7
Fous	87.1	19.1

Octant 3

Fields	Rms Error	N
Verif-Modrh	39.42	13
Verif-Fous	49.17	13

Fields	Mean	Stan. Dev.
Verif	52.1	37.1
Modrh	63.2	15.2
Fous	86.7	15.3

Octant 4

Fields	Rms Error	N
Verif-Modrh	39.37	5
Verif-Fous	32.70	5

Fields	Mean	Stan. Dev.
Verif	43.0	39.9
Modrh	29.2	5.5
Fous	66.4	20.0

Octant 5

Fields	Rms Error	N
Verif-Modrh	35.47	18
Verif-Fous	28.94	18

Fields	Mean	Stan. Dev.
Verif	44.4	37.2
Modrh	47.9	4.9
Fous	59.0	29.5

Octant 6

Fields	Rms Error	N
Verif-Modrh	23.46	18
Verif-Fous	22.78	18

Fields	Mean	Stan. Dev.
Verif	65.4	29.2
Modrh	71.9	12.0
Fous	69.6	31.2

Octant 7

Fields	Rms Error	N
Verif-Modrh	36.01	14
Verif-Fous	25.34	14

Fields	Mean	Stan. Dev.
Verif	71.7	29.2
Modrh	65.9	12.0
Fous	77.8	31.2

Octant 8

Fields	Rms Error	N
Verif-Modrh	36.92	7
Verif-Fous	47.95	7

Fields	Mean	Stan. Dev.
Verif	44.2	36.0
Modrh	30.9	6.6
Fous	64.0	23.5

(Fig. 9a), on the other hand, is only 41%, which is slightly greater than the median of the VERIFICATION data (35.5%). This octant is typically a favored location for the dry surge. The dry observations mark the dry surge which has warmed upon its recent descent from the upper troposphere/lower stratosphere. In the upstream left corner of octant 5, the verification humidity values are lower than the model humidity values. It is here that the dry surge first emerges, advancing downstream in octants 5 and 6 as the system develops. Once these regions and their extent can be systematically identified, it is possible that a bogusing scheme can be introduced that will sharpen the humidity response of the model in the specified regions.

The inside conveyor belt octants show the model's predictive skill equal to that of the LFM-II (Table 7). Even more impressive are the lower rms errors, around 23% (Table 6), for the moist half of the belt, octants 2 and 6. This indicates a significant number of moist observations occurring in an area of the conveyor belt where the dynamics conducive to upward motion are greatest. Outside the conveyor belt (Table 8) the 12-hour LFM-II forecast does slightly better with the exception of octant 8. In octant 8 the model seems to capture the drying due to subsidence better than the LFM-II, although the number of data points is too small for any reliable statistical verification.

The model's largest rms errors are found in octants 3 and 4, 39.4% in each. A frequency distribution of the data points in these two octants reveals that 80% of the observations lie below 30% or above 80%. The high rms errors actually extend down the entire right side of the belt, as again over 80% of the observations in octants 7 and 8 fall below 30% or above 80%. It is hypothesized that the large rms errors may be partly attributed to the subjectivity in drawing the ragged right edge of the conveyor belt. Another possible factor contributing to the large rms errors is the vertical

46

Table 7. Statistics for inside conveyor belt octants 2, 3, 6, and 7 of the independent data set at the 650 mb level. The data fields are identical to these of Figure 5. N is the sample size.

Fields	Rms Error (%)	N
VERIFICATION vs. MODRH	30.13	62
VERIFICATION vs. FOUS	30.70	62

Fields	Mean (%)	Standard Deviation (%)
VERIF	68.29	31.3
MODRH	72.33	14.5
FOUS	80.67	25.1
VERIF – MODRH	– 4.04	30.0
VERIF – FOUS	–12.38	27.9

47

Table 8. Statistics for outside conveyor belt octants 1, 4, 5, and 8 of the independent data set at the 650 mb level. The data fields are identical to those of Figure 5. N is the sample size.

Fields	Rms Error (%)	N
VERIFICATION vs. MODRH	35.79	48
VERIFICATION vs. FOUS	32.47	48

Fields	Mean (%)	Standard Deviation (%)
VERIF	50.13	35.1
MODRH	44.60	10.8
FOUS	66.54	26.1
VERIF – MODRH	5.53	34.8
VERIF – FOUS	-16.41	29.2

48

variability of cloud layers in the downstream and eastern portions of the conveyor belt. Here, underneath the 350 mb cirrus shield, thin layers of middle-level cloud may intrude into an otherwise dry environment. The levels at which the middle-layer clouds occur is particularly variable in octants 3 and 4. This may account in part, for the bimodal pattern of dry and moist observations found in these octants.

The downstream and eastern sections of the belt are also subject to influence by other synoptic-scale systems. Upper-level short waves and associated frontal bands that are often part of a cyclone family can precede the conveyor belt. As a consequence, the environment ahead of the developing belt can be moist, supporting clouds and possible precipitation. The cloud shields for each system are not always distinct and on occasion merge or are bridged together by a narrow band of cloud. The more common situation, however, is for the moist conveyor belt to intrude into the dry environment of an existing anticyclone, as mentioned above. This case-to-case variation may account for the large spread in the composite data. If these events can be classified into two distinct populations, with two distinct humidity structures, a modification of the model humidity pattern may be desirable.

Another model field, the 700 to 500 mb layer (7T5), was also compared against the VERIFICATION data. The model 7T5 layer is pressure weighted using 50 mb intervals from 700 to 500 mb, inclusive. It more closely approximates the FOUS layer which extends from about 490 to 740 mb. When this field was tested against the VERIFICATION data, model performance appears even better with rms errors of 31.5% for FOUS and 31.8% for 7T5.

The result at 950 mb show rms errors far smaller (for each field) than those at 650 mb. The smaller rms errors are a function of the narrowed range of humidity values present in the boundary layer. Drier values are less

49

frequent, as the boundary layer is a predominantly moist environment. This shows up well in the sample means which are very high and in the standard deviations which are very low, with the model again exhibiting the lowest standard deviation. The mean of the VERIFICATION sample is greater than that of MODRH and similar to that of FOUS for all octants together (Table 9), for inside-belt octants (Table 10) and for outside-belt octants (Table 11). No particularly strong bias is indicated by either field in the three samples.

A comparison of the rms errors between the developmental model and the observations in the dependent and indendent data sets shows that the independent data set exhibits a smaller error, 16.2%, than the dependent data set, 19.1%. Table 9 contains the results for the same statistical tests as Table 5 but for 950 mb. The model does well against the other humidity fields, scoring better than all except the 12-hour LFM-II forecast, with which it performs equally well. FOUS and MODRH performed equally well for both inside and outside conveyor belt octants, with rms errors remaining low.

Table 12 is a description of the 950 mb data in each of the eight octants comprising the model domain. Octants 2, 5 and 6 have the smallest rms errors, 13.7%, 9.8% and 11.9% respectively. Each of these octants in the developmental sample was shown to be significantly moister than each of the other five octants at the 95% confidence level. The model's humidity maximum at 950 mb is located primarily in octants 5 and 6, which in the independent sample are the octants with the lowest rms errors. Octants 5 and 6 are also the only octants where MODRH performs substantially better than FOUS, with a lower, average model rms error of 5.6%. Octants 1, 3 and 6 have model rms errors slightly larger than those of FOUS, while octants 4 and 8 have data sets too small for any meaningful interpretation.

Table 9. Statistics for all eight octants of the independent data set at the 950 mb level. The data fields consist of radiosonde observations (VERIF) and interpolated predicted values from the developmental relative humidity model (MODRH) and the LFM-II (FOUS). Parenthetical values are sample size; bracketed values are relative humidities of the horizontally flat fields.

Fields	Rms Error (%)	
VERIFICATION vs. MODRH	16.23	(113)
VERIFICATION vs. FOUS	16.16	(113)
VERIFICATION vs. SAMPLE CLIMATOLOGY MEAN	17.23	(84.1%)
VERIFICATION vs. CLIMATOLOGY	20.48	(73%)
VERIFICATION vs. RANDOM UNIFORM DISTRIBUTION	24.01	---

Fields	Mean (%)	Standard Deviation (%)
VERIF	84.01	17.3
MODRH	81.24	7.8
FOUS	83.56	15.0
VERIF – MODRH	2.83	15.9
VERIF – FOUS	.51	16.2

51

Table 10. Statistics for inside conveyor belt octants 2, 3, 6, and 7 of the independent data set at the 950 mb level. The data fields are identical to those of Figure 9. N is the sample size.

Fields	Rms Error (%)	N
VERIFICATION vs. MODRH	16.69	63
VERIFICATION vs. FOUS	15.99	63

Fields	Mean (%)	Standard Deviation (%)
VERIF	84.71	17.5
MODRH	82.54	7.7
FOUS	84.06	14.6
VERIF − MODRH	2.19	16.4
VERIF − FOUS	.65	16.1

Table 11. Statistics for outside belt octants 1, 4, 5, and 8 of the independent data set at the 950 mb level. The data fields are identical to those of Figure 9. N is the sample size.

Fields	Rms Error (%)	N
VERIFICATION vs. MODRH	15.94	50
VERIFICATION vs. FOUS	16.35	50

Fields	Mean (%)	Standard Deviation (%)
VERIF	83.37	17.1
MODRH	79.62	7.6
FOUS	83.02	15.5
VERIF – MODRH	3.75	15.3
VERIF – FOUS	.35	16.5

53

Table 12. A statistical description of the eleven case independent data set at the 950 mb level. The data fields for each of the eight octants comprising the model domain are identical to those of Figure 9. N is the sample size.

Octant 1

Fields	Rms Error	N
Verif-Modrh	16.41	19
Verif-Fous	15.87	19

Fields	Mean	Stan. Dev.
Verif	82.6	16.9
Modrh	78.3	5.2
Fous	90.8	9.4

Octant 2

Fields	Rms Error	N
Verif-Modrh	13.74	22
Verif-Fous	11.99	22

Fields	Mean	Stan. Dev.
Verif	86.0	13.4
Modrh	84.1	6.3
Fous	86.1	12.8

Octant 3

Fields	Rms Error	N
Verif-Modrh	24.68	13
Verif-Fous	22.27	13

Fields	Mean	Stan. Dev.
Verif.	78.1	27.0
Modrh	72.8	7.7
Fous	85.5	12.3

Octant 4

Fields	Rms Error	N
Verif-Modrh	24.37	5
Verif-Fous	7.73	5

Fields	Mean	Stan. Dev.
Verif	80.7	21.7
Modrh	63.4	3.8
Fous	76.6	16.2

Octant 5

Fields	Rms Error	N
Verif-Modrh	9.81	18
Verif-Fous	15.42	18

Fields	Mean	Stan. Dev.
Verif	84.3	16.6
Modrh	85.8	3.2
Fous	79.8	18.8

Octant 6

Fields	Rms Error	N
Verif-Modrh	11.93	18
Verif-Fous	17.69	18

Fields	Mean	Stan. Dev.
Verif	85.6	16.1
Modrh	89.7	3.2
Fous	79.5	18.8

Octant 7

Fields	Rms Error	N
Verif-Modrh	15.74	14
Verif-Fous	12.06	14

Fields	Mean	Stan. Dev.
Verif	87.7	16.1
Modrh	81.9	1.8
Fous	84.8	18.5

Octant 8

Fields	Rms Error	N
Verif-Modrh	19.00	8
Verif-Fous	21.97	8

Fields	Mean	Stan. Dev.
Verif	84.2	18.7
Modrh	79.0	3.4
Fous	77.6	11.1

If the developmental humidity model is to be considered as an operational aid, its performance must be judged with respect to that of current techniques. The performance of the model in the independent test is weak but somewhat encouraging. Root-mean-square errors of the LFM-II 12-hour forecasts of relative humidity were close to those of MODRH, with an absolute difference of less than 1% at 650 mb and 0.1% at 950 mb.

These 12-hour forecasts were for land regions where many radiosonde observations were available to tune the initial analyses. Considering that radiosonde observations are sparse over ocean regions, it is expected that LFM-II initial analyses are not as good there, with a consequential forecast deterioration. Hence, it is expected that MODRH, nearly as good over land, might gain on an LFM-II forecast over open ocean. When the rms errors of MODRH and another possible first-guess field, climatology, are compared, the model does far better, showing an absolute difference of 5% at 650 mb and 4.3% at 950 mb.

III. Factors Related to the Evolution of Small-scale Cloud Vortices in Polar Airstreams Over the Northern Oceans[1]

1. Background

Over the high latitude ocean in winter, small-scale cloud clusters are often observed to develop within cold air masses. These features sometimes develop enough rotation to evolve into a polar low. They are found within a polar airstream as a post-frontal phenomenon and are an interesting exception to the Norwegian cyclone model. A number of researchers have performed case studies of developing polar lows, and there is debate regarding the relative roles played by CISK and baroclinicity in these developments (Harrold and Browning, 1969; Rasmussen, 1979; Reed, 1979; Mullen, 1979; Sardie and Warner, 1983).

As noted by Rasmussen (1979), however, an examination of a sequence of satellite pictures over an extended period reveals that there are several types of cloud configurations that can evolve into, or be associated with, a polar low. This suggests that polar lows may develop in different ways. Indeed, there are different cloud configurations associated with the various cold-air cyclones or polar lows reported in the literature (Seaman et al., 1982). Accordingly, this section has three purposes: (1) to document, in a systematic way, the range of vortices; (2) to indicate which of these cloud configurations are accompanied by significant pressure perturbations; (3) to present preliminary results of a study to determine if there are systematic differences between the synoptic-scale environments of cold-air vortices which undergo development and those which remain insignificant.

---

[1]This chapter was previously produced in slightly different form in the Preprint Volume of Extended Abstracts: Conference of Cloud Physics, Nov. 15-18, 1982, Chicago, IL, published by AMS, Boston, MA.

2. Types of cloud configurations accompanying cold-air vortices

Europe experienced a rather cold December, 1981, in relation to cold air aloft accompanying a persistent mid-level trough with axis over Scandinavia. Accordingly, with the trough axis to the east and the polar front jet driven far to the south, the period from early December through early January was ideal for a study of cold-air vortices. A systematic study was performed for the period from 1 December 1981 through 5 January 1982, over oceanic areas and adjacent continental regions from 35N to 75N and roughly from Greenland to Europe and Scandinavia (54W to 45E). The Mediterranean region was excluded. Figure 14 shows the frequency of cold-air vortices by "box" (5 degree latitude by 5 degree longitude area).

Imagery from each pass of the NOAA-6 and NOAA-7 satellites was inspected for the existence of mesoscale cloud configurations, initially independently of other data. Because of the relative infrequency of visible imagery at the northern latitudes during winter, the study was based primarily upon infrared images (which were unenhanced). If a mesoscale cloud system showed signs of circulation at any time, it was counted as a cold-air vortex and its path was charted from the time circulation first appeared until its demise. Vortices evolving from or associated with a recognizable synoptic-scale frontal band or conveyor belt were excluded from the study, as these vortices did not qualify as cold-air phenomena.

Once all the cold-air vortices occurring on a particular day were identified in satellite imagery, surface charts were consulted in order to determine the magnitude of the pressure perturbation accompanying each vortex. In order to estimate the pressure deficit between the mesoscale vortex and its synoptic scale surroundings, sequences of charts were consulted to identify the temporal changes in sea-level pressure as a vortex passed a

57
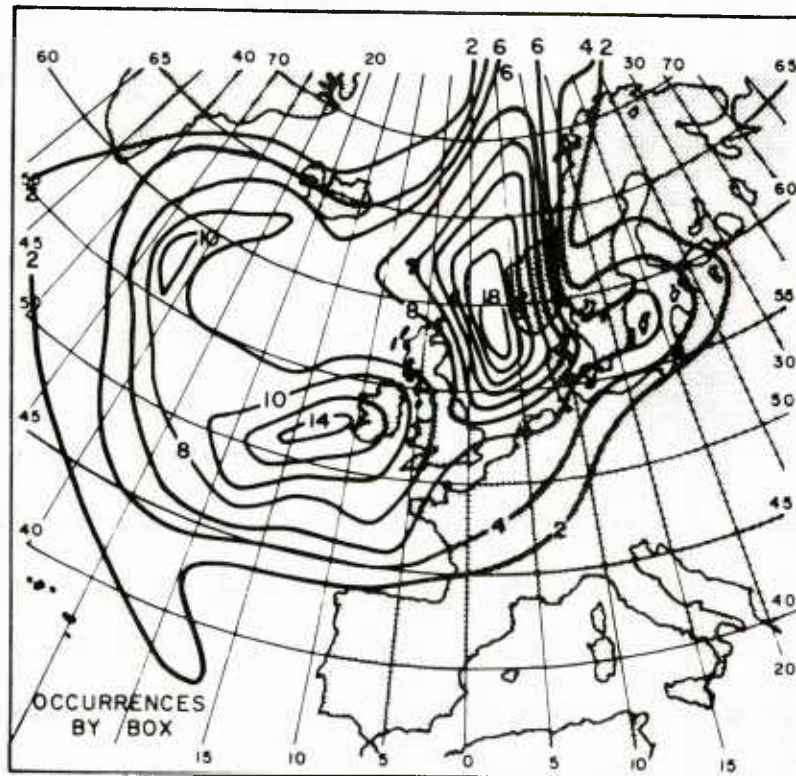
Figure 14.   Frequency of occurrence of cold-air vortices of all types,
             1 Dec 1981 – 5 January 1982.

station. Further, smoothed (synoptic scale) isobaric patterns were drawn on charts at times when vortices were passing over observation stations. An estimate of deficit pressure was obtained by comparing the value of the observed pressure to that expected from the smooth synoptic analysis. When a vortex did not encounter a station and neither of these techniques could be applied, no deficit pressure value was assigned. Where possible, deficit pressures were estimated and tabulated at 12-hour intervals (0000 and 1200 GMT).

Nine categories of cloud configurations were observed, as indicated in Table 13. Table 13 also lists for each category: (a) the total number of observations (one observation per vortex per 12-hour period), (b) the number of observations when deficit pressure estimates were available, and (c) the mean and standard deviation of the deficit pressure. A further breakdown of the cloud category-deficit pressure relationship is given in Table 14.

Category 1 vortices were the most sensational and occurred in several different forms: weak commas; strong, classic commas; spiral configurations of deep convection; "instant commas" of deep cirrus-topped cloud developing suddenly from a virtually cloud-free environment; and occluded commas in which only streaks of narrow convection identify the circulation center, but the deep cloud shield persists to the northeast. Many of the polar lows in the literature are of one of the category 1 forms (Harrold and Browning, 1969; Lyall, 1972; Monteverdi, 1976; Reed, 1979; Mullen, 1979; Seaman et al., 1982).

Category 2 vortices were also significant in terms of deficit pressure, but were quite different in configuration. A descriptive name of "merry-go-round" is suggested, as the vortex is comprised of several deep bands revolving about a relatively cloud-free center.

59

TABLE 13

OBSERVATIONS BY CATEGORY OF CLOUD PATTERN

CATEGORY	DESCRIPTION	TOTAL # OBS	# WITH ΔP	MEAN ΔP
1	COMMA, DEEP SPIRAL	84	54	10.1 ± 6.1mb
2	"MERRY-GO-ROUND" OR RING OF VORTICES	3	3	8.7 (± 3.2)
3	CRESCENT	17	13	3.5 ± 2.4
4	OVAL, SOLID MASS	10	3	5.7 (± 1.2)
5	MULTIPLE DEEP BANDS	108	34	4.0 ± 2.3
6	MULTIPLE SHALLOW BANDS	36	12	3.5 ± 2.2
7	SINGLE DEEP BAND	2	2	4.0 (± 1.4)
8	SINGLE SHALLOW BAND	1	1	0.0
9	SWIRL IN CUMULUS STREETS	72	26	2.9 ± 2.1
STRONG COMMA	(DIAMETER > 3.6 DEG LAT OR > 0.5 REVOLUTION)	44	27	12.7 ± 6.6
WEAK COMMA	(DIAMETER < 3.5 DEG LAT AND < 0.5 REVOLUTION)	40	26	7.0 ± 3.5

TABLE 14

RELATIONSHIP BETWEEN CLOUD CATEGORY AND PRESSURE PERTURBATION

CATEGORY	# OBS WITH ΔP	>2	>4	>6	>8	>10	>12	>14	>16	>18	>20	RANGE
1	54	100%	93%	74%	56%	37%	33%	28%	24%	20%	13%	2 - 23
2	3	100	100	67	67	67	0	0	0	0	0	5 - 11
3	13	77	46	23	0	0	0	0	0	0	0	0 - 7
4	3	100	100	33	0	0	0	0	0	0	0	5 - 7
5	34	79	56	29	6	0	0	0	0	0	0	1 - 9
6	12	75	50	17	0	0	0	0	0	0	0	1 - 7
7	2	100	50	0	0	0	0	0	0	0	0	3 - 5
8	1	0	0	0	0	0	0	0	0	0	0	0
9	26	73	27	12	8	0	0	0	0	0	0	0 - 8
STRONG COMMA	27	100	100	85	67	56	48	44	44	37	22	4 - 23
WEAK COMMA	26	100	85	62	42	15	15	8	0	0	0	2 - 14

The rest were notably weaker, with respect to deficit pressure. The vortices behaved somewhat similarly, in terms of deficit pressure, to both tropical cloud systems or oceanic mid-latitude cyclones. Curved, banded convective configurations had deficit pressures that were generally largest when the convection was in the form of a broad cluster of deep, large-diameter elements and the bands made considerable fractions of a full revolution about the circulation center. This is similar to the behavior of tropical storms (Dvorak, 1975). The vortices with more stratiform appearances seemed to generally follow the guidelines of Junker and Haller (1980) for oceanic cyclones: the deficit pressure increased as the deep cloud system became progressively a spiral, as a deep band revolved about the circulation center. The rate of increase of deficit pressure appeared to be only half of that specified by Junker and Haller, however, and was also a function of diameter of the circulation. Strong commas, having either large circulation diameter or a band spiralling more than a half revolution about the circulation center, had significantly larger deficit pressures than weak commas (at the 0.1% confidence level).

3. Stratification by rate of change of configuration

Vortices were also subjectively classified by the rates at which the circulation diameter and band revolution increased with time. A vortex was given only one classification according to its dominant behavior. Non-developing vortices were called steady if they appeared to be significant in terms of moderate amounts of circulation and moderate diameters, and as weak or insignificant if they were shallow, ill-developed, or short-lived. Significant commas, which were only observed during dissipation stages (satellite imagery not available for early stages) were classified as dissipating commas.

62

Despite being subjective, the growth classification was remarkably accurate, when compared to deficit pressures. Table 15 summarizes the observations of each vortex by its nature. Since developing vortices had longest lives, and spent only a portion of their lives in the mature stage, the mean deficit pressure shown is considerably less than the peak values and the standard deviation is large. Developing vortices had deficit pressures which exceeded 8 mb sometime during their lifetime, whereas steady vortices did not. Steady vortices had deficit pressures which leveled off near 5 mb, whereas insignificant vortices did not attain 5 mb deficit pressures.

Table 16 relates cloud configuration category to the classification of the vortex. Commas and the merry-go-round were normally significant, whereas shallow features category (6 and 8) and cumulus street swirls (category 9) were normally insignificant. Steady vortices tended to fall in the intermediate categories (with moderate deficit pressures). Thus, cloud configuration category, pressure deficit, and growth classification are strongly associated, and may be inferred with some skill from satellite imagery.

4. Synoptic environment of vortices of different nature

In view of the interest in determining the mechanism for the development of polar lows, a study was conducted to compare the synoptic-scale environments of these vortices, as stratified. The basic question is whether there are differences on the synoptic scale between vortices of different classification, or whether the sub-grid-scale processes of latent and sensible heating are crucial.

Analysis fields from the operational model of the ECMWF (European Centre for Medium Range Weather Forecasts) were used, and objective calculations were made at 12-hour intervals of various kinematic, dry thermodynamic, and dynamic

63

TABLE 15

OBSERVATIONS BY CLASSIFICATION OF VORTEX

CLASSIFICATION	ESTIMATED # CASES	ESTIMTED # OBS	# OBS WITH ΔP	MEAN ΔP
DEVELOPING COMMAS	16	101	61	9.6 ± 6.0
STEADY	18	73	42	4.8 ± 1.8
INSIGNIFICANT	96	155	41	2.1 ± 1.7
DISSIPATING COMMAS	3	10	4	4.0 (± 2.5.)

TABLE 16

RELATIONSHIP BETWEEN CLOUD CATEGORY AND VORTEX CLASSIFICATION

(PERCENT OCCURRENCES)

CATEGORY	# OBS	SIGNIFICANT (DEVELOPING OR DISSIPATING COMMA)	STEADY	INSIGNIFICANT
1	84	79%	21%	0%
2	3	100	0	0
3	17	47	24	29
4	10	40	10	50
5	108	19	26	55
6	36	0	33	67
7	2	0	50	50
8	7	0	0	100
9	72	13	13	74
STRONG COMMA	44	91	9	0
WEAK COMMA	40	65	35	0

parameters listed in Table 17. A grid distance of 450 km was chosen for these calculations, consistent with the density of upper-air observations. The ECMWF analyses normally do not reveal mesoscale features (such as polar vortices) in these regions, as bogusing on the basis of satellite imagery is not performed.

Values of numerous parameters were calculated with respect to the centers of circulation of the vortices, composited, and stratified by the vortex classification. Two statistical comparisons have been performed, using observations during only early stages of the vortex lifetime (first 18 hours) and using all observations. Table 17 presents results for the early-stage comparisons. Checks indicate differences in means (with respect to the developing vortices) that are significant at the 5% confidence level. Other parameters (not listed) were not significant at the 5% confidence level. There were no significant differences between the steady and insignificant vortices at this stage.

Developing vortices originated at more northerly latitudes, resulting in colder sea-surface temperatures and larger absolute vorticities. There is some suggestion that convergence of 850 mb absolute vorticity (the relative vorticity difference was not significant) by inflow to the disturbance may have been a significant factor in the initial development. Developing vortices occurred with lower windspeeds, and with colder temperatures at 500 mb. Steady vortices showed negative advection of thermal vorticity by the thermal wind at 500 mb. In the initial stages the developing vortices moved significantly to the right of the instantaneous 700 mb thermal wind and 1000-500 mb wind shear vectors. This characteristic did not continue and, in fact, the developing vortices moved to the left of the 1000-500 mb shear vector when deviant movement was averaged over the entire lifetime. Non-developing vortices continued their small rightward movement throughout.

65

TABLE 17

SIGNIFICANCE RESULTS - INITIATION STAGE

PARAMETER	DEVELOPING	STEADY	INSIGNIFICANT
Sea Surface Temperature (°K)	278.6 ± 2.4	√280.5 ± 2.5	√280.3 ± 2.6
500 mb Temperature (°K)	235.9 ± 5.3	236.0 ± 6.1	√238.8 ± 6.7
700 mb Geostrophic Windspeed (m s^{-1})	6.8 ± 4.5	9.7 ± 5.1	√ 9.6 ± 5.6
850 mb Absolute Vorticity (10^{-5} s^{-1})	14.7 ± 1.6	13.9 ± 2.8	√ 13.3 ± 2.8
500 mb Thermal Vort. Adv. by Thermal Wind (10^{-17} s^{-2})	0.7 ± 1.6	√-0.7 ± 1.5	+0.0 ± 2.3
Lapse Rate, 700-500 mb (°K km^{-1})	7.1 ± 1.1	6.7 ± 0.8	√ 6.7 ± 0.8
Average Windspeed, 1000-500 mb (m s^{-1})	7.8 ± 5.8	11.9 ± 6.1	√ 11.2 ± 6.7
Average Windspeed, 1000-500 mb (m s^{-1})	7.1 ± 4.3	10.2 ± 6.0	10.0 ± 6.0
Average Temperature, 1000-500 mb (°K)	254.6 ± 3.5	254.5 ± 5.9	√257.0 ± 5.7
Deviation of Movement from 700 mb Thermal Wind (deg az.)	66 ± 87·	51. ± 91.	√ 25. ± 68.
Deviation of Movement from 1000-500 mb Geostrophic Shear (deg az.)	65 ± 88.	47. ± 86.	√ 19 ± 73.

It should be noted that the cold-air vortices, in general, were accompanied in early stages by cold temperatures, low heights and thicknesses, considerable temperature gradients and sea-surface temperature differences, positive relative vorticity, weak positive advections of absolute vorticity and thermal vorticity, weak cold advection, and weak conditional instability below 700 mb. The early movement was roughly with the 700 mb geostrophic wind. Whereas mean values of these parameters at the vortex centers were probably significantly different from climatological mean values for the region, differences of these parameters between vortices of different natures in early stages were only significant where noted above.

All of the parameters showing differences during early stages also showed significant differences of the same sign when all observations were used, except for deviant movement. Additionally, a number of other parameters showed significant differences when all observations were used. Presumably this was a result of one or more factors, including: (1) larger sample sizes; (2) large circulations accompanying the developing vortices in their mature stages affecting synoptic analyses; (3) different processes becoming significant as the vortices evolved. Whatever the implications of the greater number of discriminators over the life of the events, the occurrence of high vorticity air with unstable lapse rate in cold air that is colder than the underlying sea, moving at slow to moderate speed, appear to be necessary for these vortices. Regions of warmer air moving faster and having less vorticity appear to be less promising.

5. Lake vortices

To gain further insight into formative mechanisms, fourteen wintertime mesoscale vortices over the United States Great Lakes were studied. These had

67

diameters of 50 to 120 km and cloud tops as high as 5.5 km. In contrast to
the oceanic variety, all of these vortices were rather innocuous, associated
only with weak cyclonic wind circulations and brief snow showers, though there
are reports (Hjelmfelt et al., 1983) that more extreme cases occasionally
occur.

Shoreline-parallel cloud bands occurred over the lakes (Michigan,
Superior and Huron) during many of the vortex developments, and some of the
vortices were initiated as small disturbances along these bands. These
initial disturbances were rather small, however, and the developing lake
vortices quickly grew to diameters approaching the width of the lakes. This
suggests that vorticity production associated with diabatic heating over the
lake was more important for lake vortex development than the vorticity-
generation processes operating on the scale of the shoreline-parallel cloud
band.

Lake vortices occurred in cold air masses and near or just east of a
high pressure ridge, but synoptic-scale processes otherwise did not appear
to contribute to lake vortex development. Positive vorticity advection and
positive (warm) thermal advection, favoring synoptic-scale cyclogenesis, were
not normally present.

Though many of the vortices showed little systematic movement, three of
the vortices (on 28 February 1980, 8 January 1981, and 6 March 1981)
translated not only over portions of Lake Michigan but also moved inland.
Whereas this might suggest some connection to a traveling synoptic-scale
disturbance, it may have been merely a shift in the steering wind direction.
In two cases, warming of the air over land in the afternoon reduced the
air-water temperature difference. It is suggested that the vortices were
generated and maintained over the lake during the morning by the stationary

pattern of diabatic heating, and were steered inland by the synoptic-scale flow in the mid-to-late afternoon when this forcing weakened. Indeed, the vortices themselves weakened rapidly during their movement inland.

It appears that the lake vortices may be similar to the weakest class of vortices that form near the shores of Greenland, Iceland and Norway, but they do not have the long residence times over warmer water that the well-developed polar lows enjoy. Thus, they do not get much opportunity to spin up. It is of interest, however, that this class of event seems to occur only in synoptically benign environments.

Chapter IV. Diagnosis and Predictions Related to Meteorologically Active
            Boundaries

1. Boundary locator

In recent years, the availability of geostationary satellite imagery at
relatively high frequency and spatial resolution has stimulated a resurgence of
interest in the formation of clouds and precipitation along boundaries at all
scales (Purdom, 1976; Forbes et al., 1982), reemphasizing the ideas of Fujita
(1963). Indeed, the perception that much hydrometeorological activity occurs in
association with boundaries of all spatial scales has only made the forecaster's
task more difficult. Not only is there more to consider and look for, but the
available analyses are not designed to help very much at small scales. The
emergence of computer graphics systems supporting real-time weather station
operations gives the forecaster some help in identifying potentially significant
boundaries quickly. Many such boundaries are quite subtle, especially in the warm
season, consisting of dew point "fronts" or the like.

We have taken an idea from Clarke and Renard (1966) which is currently in use
at the Fleet Numerical Oceanographic Center and extended and modified it for use
in situations where moisture patterns are significant. Where Clarke and Renard
use the gradient of the gradient of potential temperature (GGθ in Navy usage) to
locate "pure and clear, temperature and density phenomena", we prefer to locate
active or potentially active boundaries in the sense of hydrometeor location.
Thus, we use the wet bulb potential temperature (as Environment Canada has done)
and performed some of Renard's operations, as well as vertical checks based on
vorticity gradients. Huber-Pock and Kress (1981) have suggested a thickness
humidity index and a frontal activity index for the objective front location work
currently done in Austria which is based on similar reasoning. However, we prefer
to avoid geostrophic arguments or any approach that is most applicable to the

70

synoptic scale. As a practical matter, our method is probably most useful for mesoscale phenomena over the eastern two-thirds of the United States in the warmer seasons, but it should also have value over the oceans, if data are available.

We use the surface value of the wet bulb potential temperature (θ_w) and apply the following steps.

(a) Produce an analysis of surface θ_w on a 30 by 40 grid. This is done by interpolating approximately 450 surface hourlies to the grid and smoothing, then using this analysis as a first guess to a Cressman analysis, then smoothing that with 3 passes of a 1:4:1 smoother.

(b) Calculate the magnitude of the gradient of θ_w on the grid. Depending on the map background used, Δx is of the order of 40-80 km, because a 30 x 40 grid is always used. Centered differences over 2 grid lengths are employed.

(c) Calculate the magnitude of the gradient of the scalar gradient value found in step (b).

(d) Calculate the Laplacian of θ_w in the conventional way, using a 4 grid length spacing.

(e) Scan each of the 1200 points of the gradient of the gradient of θ_w at each of the grid points. Retain those values of the gradient of the gradient where the Laplacian is negative and set the other values to zero. Since the Laplacian should be negative in θ_w maxima (warm tongues), this has the effect of locating the warm side of the θ_w gradient, which is often the site of interesting weather. The resulting field is an elongated one which has its largest values stretched along the warm moist side of a gradient of θ_w. By contouring the field, one can get a quick map of these locations.

(f) Perform an upper air check at 0000 GMT and 1200 GMT (and possibly at hours close to those times). We calculate the gradient of relative vorticity at 850 mb on a 30 by 40 grid using centered differences over 2 grid lengths. The

71

method of analyzing the winds is similar to that used for surface θ_w, except that the radii of influence are larger because upper air coverage is less dense. It is well known that fronts normally manifest cyclonic relative vorticity values; Hoskins and West (1979) have published several examples of relative vorticity patterns from a model that match commonly encountered frontal cloud patterns rather well. The vorticity that can be caluclated from radiosondes is however synoptic scale; its gradient is used here to locate boundary zones aloft, in the manner suggested by S. Simplicio (personal communication). Mesoscale vorticity values would be preferable. In the present case, we are simply checking for vertical support for the significant gradient and are not performing a hydrostatic check on a "front". Accordingly, the existence of any vorticity gradient at 850 mb of approximately 3×10^{-5} sec^{-1} over 100 km within approximately 225 km in any direction is considered as evidence of vertical support for the feature in question.

(g) Scan along the grid rows and columns of the field to find a one-dimensional maximum of the gradient of gradient θ_w whether or not the upper air check is done. For some experiments a positive Laplacian of sea level pressure is used to eliminate ridges and highs. In our displays, the points that satisfy these criteria are displayed as asterisks and we sometimes connect them with simple line segments. If an upper air check has been performed (0000 or 1200 GMT) we display W's for boundaries with upper vorticity support and S's for unsupported boundaries. We expect these two types of boundaries to behave differently with respect to hydrometeor activity.

Figure 15 shows the principal features of the surface map for 1200 GMT 22 July 1981. A 1022 high, centered over Lake Superior had spread cool, dry air over much of the eastern United States; the position of the associated front as seen on the National Meteorological Center (NMC) analysis is shown in Fig. 15. Two weak
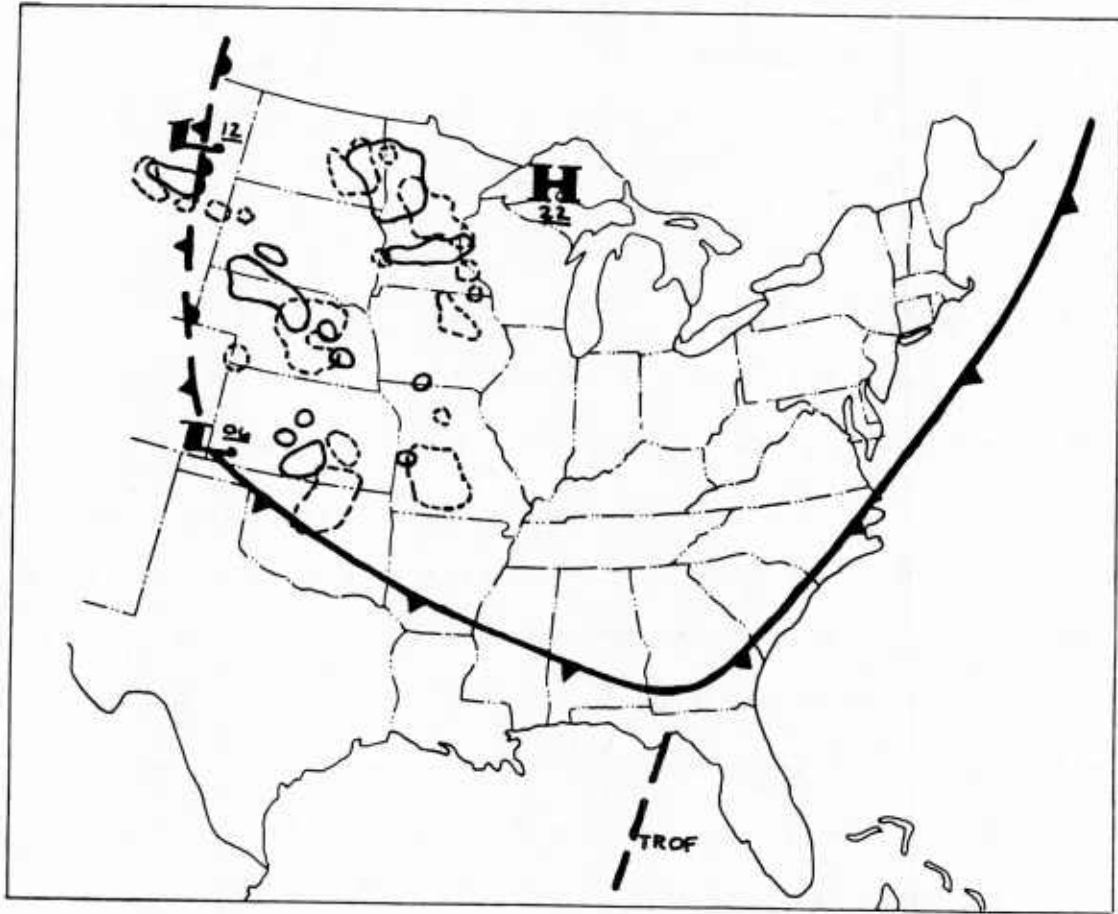
72

Figure 15.   Surface map, 1200 GMT 22 July 1981.

cyclones were located in a frontal zone on the High Plains, with centers in eastern MT and southwest KS. A weak trough was present in the eastern Gulf. Also depicted on Fig. 15 are the composite manually-digitized radar (MDR) reports for both 1135 GMT (solid) and 1435 GMT (dashed). Several zones of activity were present, with major clusters of showers and thundershowers moving east-southeastward from eastern ND and MN, from the SD-NE border regions across ME, and from KS to OK during the 3-h period. In addition, a major cell grew in MO. All of these were well east of the analyzed surface front position. Some cells, mainly offshore of the Gulf Coast, are not shown in Fig. 15.

An analysis of surface wet-bulb potential temperature at a 1°C contour interval is shown as Fig. 16 and while this chart makes it easier to detect the principal gradient and some regions of enhanced local gradient, it is still not wholly obvious where to locate the meteorologically significant boundaries.

Figure 17, also valid at 1200 GMT, shows the points that have passed the tests a-g (but without the sea-level pressure test). A similar map (without the upper air check) can be available on our system at about H + 15 for any hour during the day. All points which passed the upper air check, are labeled W; unsupported boundaries are labeled S.

It can be seen that there is considerably more detail present in the BL (boundary locator) than is usually available. What is more, the detail seems to relate rather well to the reported shower patterns, for the supported (W) boundaries. The line from extreme eastern ND through MN, IA and MO to LA is close to one of the shower/thundershower bands. The boundary from eastern WY to northern MO lies parallel to, and just on the cold side of the cells moving across NE. This band appears to act somewhat like a warm front. Of particular interest, a vigorous cell, with a top at about 14 km, grew in MO during the 3-h period, not far from the intersection of these two boundaries. Also, the KS-OK boundary was
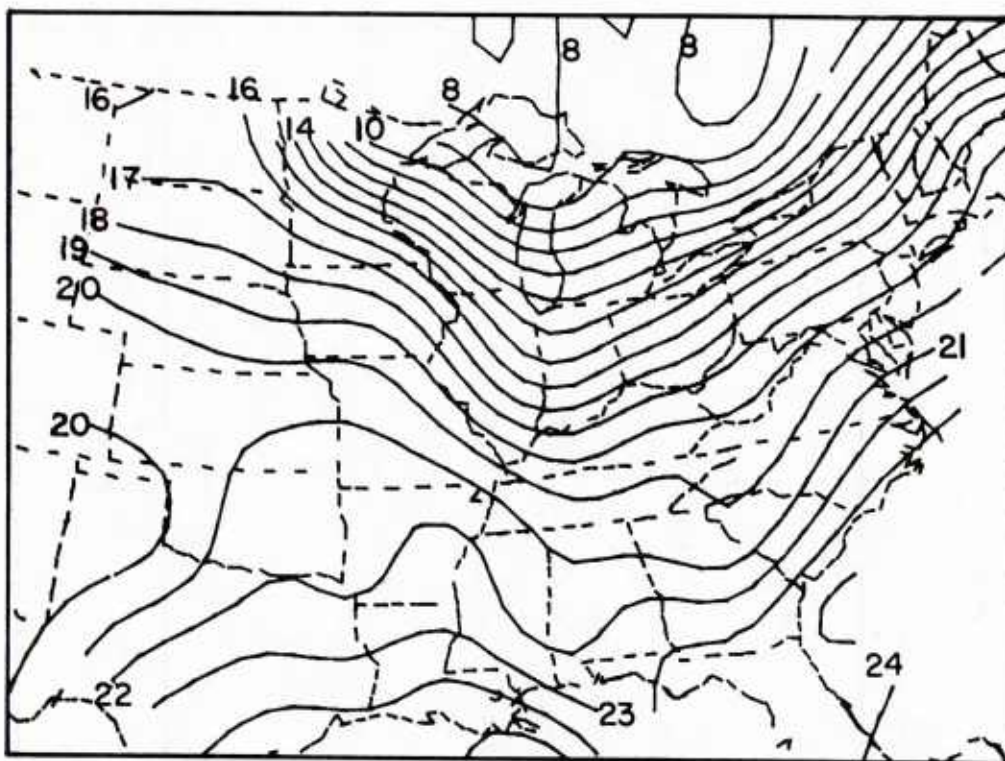
74

Figure 16.   Surface wet-bulb potential temperature (°C) 1200 GMT 22 July
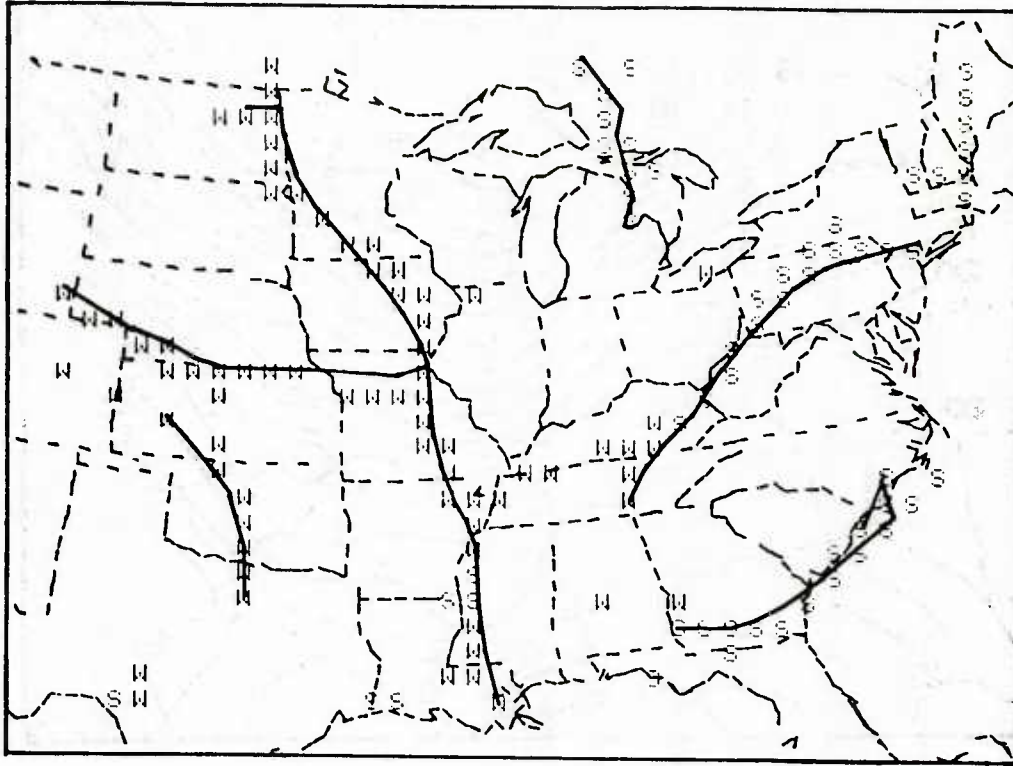   1981.   Contour interval 1°C.

Figure 17.   Locations of boundaries based on the data of Fig. 16. W implies
upper level support, S the lack therof.

active. In contrast, none of the boundaries labeled S on Fig. 17 were active, nor did they become so during the day, with the single exception that the S boundary in northern FL exhibited afternoon thunderstorms as the convection shifted onshore, as it typically does during the daytime. Also, the extension of the ND-MO-LA boundary did not become active along the MO-LA segment, despite some upper support and despite being in the surface "front" region of a pressure trough. Indeed, no other regions on this map had activity this day. The BL field over-specified the regions of the potential activity.

To reduce such over-specification somewhat, we also apply another test, which attempts to mask out regions of anticyclonic surface isobars by checking the sign of the Laplacian of sea level pressure. Figure 18 shows the result of that step. Much of the weak boundary region in anticyclonic conditions (which did not produce showers, but did have cloudiness maxima) is suppressed, and the supported boundaries mostly remain. Isolated pockets, which did not produce showers remain, however, in AR, MS, TN, KY, eastern PA, NJ, and New England. There is still much for the forecaster to do.

Nevertheless, these BL fields appear to have had some diagnostic value. They exhibit good time continuity in the hourly (unchecked for upper support) versions and they seem to make sense. Masking with the Laplacian of surface pressure is sometimes helpful, but often isn't necessary. In any case, the BL fields appear to be more helpful than conventional maps in alerting the forecastern to the existence of possibly significant boundaries.

2. Forecasting experiment

To test the application of the boundary locator in a real-time forecasting environment, the following experiment was performed. Six senior students, who had taken essentially all of the required courses for undergraduates and who had displayed an interest in forecasting (through such activities as the student-run
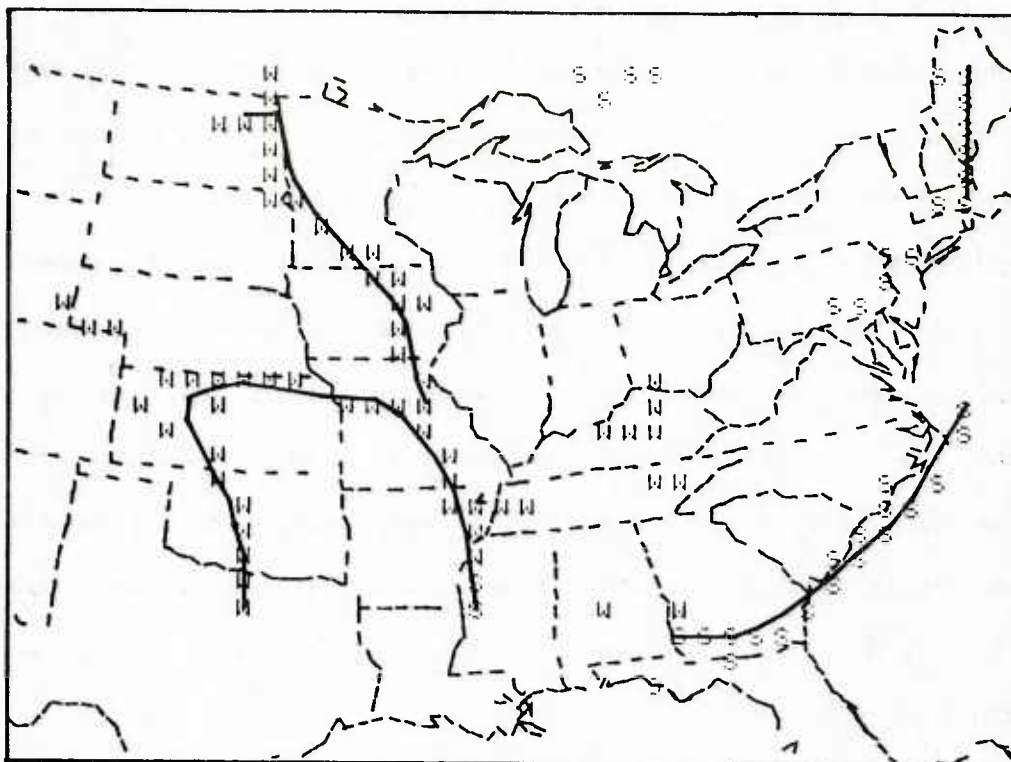
77

Figure 18.   Locations of boundaries based on the data of Fig. 16 with regions of anticyclonic sea-level isobars suppressed.

Campus Weather Service) each made convective shower forecasts on twenty different late spring days. The objective was to identify, with a 5.5 hour lead-time, which of 30 2 x 2 deg. latitude boxes would contain afternoon radar echoes, as reported on the 2135 GMT Manually Digitized Radar (MDR). Forecasts were due at 1600 GMT (local noon). Each forecaster had about 10 opportunities to use the real-time interactive computing system, which presented the opportunity to locate bounaries objectively and to make other calculations as he or she desired. In addition, each forecaster made an equal number of forecasts using conventional techniques. On most days, more than one forecaster was in each position. Thus, there was a set of forecasts made on 24 different days that comprised YES/NO forecasts for 1890 2 degree latitude by 2 degree longitude boxes in which the interactive computer system was used, and 1860 control forecasts for the same days and boxes made by the same individuals (but on different days than when the individual concerned was in the computer position of the course) where the computer system was not used. Forecasters were encouraged, but not required, to use the boundary locator. In this way the forecasters provided their own control, and since they were scrambled back and forth into the two positions so that each would do a like number of computer and control forecasts, the effects of prior forecaster skill differences are minimized. It is possible, of course, that an individual might hit all "easy" days in one position and all "difficult" days in the other, but their scheduling was made random initially, then controlled to balance the number of opportunities. One can never be sure in scheduling human beings whether all possible biases are cancelled. The disparity between 1860 and 1890 shows that perfection was not achieved.

Table 18 shows the results of the experiment. Measures of success that are tabulated include mean percent correct in labeling active or inactive boxes, together with the standard deviation of the numerator, the number of correct

79

TABLE 18.

May Forecasting Experiments

N = 24 days x 30 boxes

METHOD	% CORR	ST DEV (# Boxes)	THREAT	BIAS
CLIMO (18 boxes)	51	–	0.42	1.05
ALL YES	58	–	0.58	1.73
PERSIST	65	(5.7)	0.42	0.51
SMART PERSIST	70	(4.7)	0.54	0.77
NMC MAP	58	(7.9)	0.33	0.45
BL RAW	61	(3.6)	0.52	1.09
LAP SLP	66	(5.4)	0.50	0.83
DIV SFC	66	(5.1)	0.50	0.78
VORT SFC	66	(4.7)	0.51	0.81
MRH 45	68	(4.1)	0.54	0.87
HUMAN W/RAW BL (N = 1890)	78	(3.7)	0.66	0.94
HUMAN CONTROL (N - 1860)	78	(4.0)	0.67	0.90

boxes. Also shown are threat scores (critical success index) which is the ratio of the YES/YES box in a 4-box contingency table to all events except the NO/NO box. Threat scores must always be interpolated in the context of any related bias, with numbers greater than one implying over-forecasting and numbers less than one, underforecasting. Overforecasting improves threat scores. Other measures, such as skill scores, were calculated and show a similar result.

For comparison and interpretation, a number of standard forecasts were prepared and scored, along with some purely objective forecasts. Among standard forecasts, climatology, the normal 2130 coverage assigned randomly, does least well (forecasting showers for every box is somewhat better, if heavily biased). Persistence of the 1535 GMT morning radar pattern is better still, but understates the coverage, as would be expected. For this reason, a "smart" persistence, in which any box having a 1535 GMT echo plus any adjacent boxes to the north or east that did not have echoes were treated as "yes" forecast boxes, to allow for daily expansion and the usual motion of echo patterns in disturbed regions (northeastward). This method can be taken as the level of no skill that a meteorological approach should defeat.

Objective yes forecasts were made for any box having an NMC front or being immediately adjacent to a box containing a front (NMC MAP); if the boundary locator was in or adjacent to a box (BL RAW); and to various combinations of 1500 GMT surface predictors, calculated on a 30 x 40 grid having a spacing of about 60 km. In particular, LAP SLP means that if a boundary locator box or adjacent box had a negative Laplacian of sea-level pressure, a yes forecast was made. Negative surface divergence (DIV SFC) produced a yes forecast only for boxes adjacent to or displaying a boundary locator and having convergent surface winds. Similarly, positive surface vorticity and an analysis of 1000-1500 mean relative humidity based on surface observations of cloudiness and rain were combined with

81

the boundary locator to make selections. The humidity discriminator was used for points estimated to have mean humidity greater than 45 percent.

It can be seen that the objective forecasts were better than the simple standards, but could not beat the smart persistence. Only human beings could. And, interestingly enough, the humans did it equally well in either computer-aided or their control positions!

It is difficult to interpret these results in any other way than to say that these forecasters did an excellent job on the stated problem. They correctly labeled nearly 4 of every 5 boxes, which means that they correctly pictured the synoptic meso-α scale pattern of showers rather well. Threat scores of 0.66 are excellent, as well, implying only a slight mismatch in pattern placement. Especially notable is the small dry bias. A small increase in forecast frequency would eliminate the bias and improve the threat scores slightly.

It certainly cannot be concluded that the boundary locator helped. Whether the forecasters learned from its use can only be speculated, but it seems most likely that good forecasters arrive at their conclusions by many different paths and from different data and fields.

3. Objective composites of surface fields related to strong rains

In order to develop more techniques for generating objective guidance for predicting strong convection on the basis of surface observations, a compositing experiment embodying moisture convergence along boundaries was performed. In this experiment, the the atmosphere over the eastern U.S. was studied for thirty summer days. Surface fields from 1200 GMT and 1500 GMT were analyzed together with some upper air data from 1200 GMT. An attempt was made to identify predictors of rainfall amounts greater than 1.27 cm during the subsequent 1800-0000 GMT 6-h period. Rainfall observations were as reported over teletype circuits, which greatly understates the rain frequency, but also understates the no-rain frequency. The effects do not cancel, so this effort can be thought of as a

pilot project. Much detail is available in a thesis by Mr. Arthur Person, dated May 1983. Only a few highlights are mentioned here.

One interesting analysis point occurs where there is negative moisture divergence (convergence) along a boundary, as determined by the objective boundary locator. These fields can be calculated hourly. Moisture convergence has been shown to be a valuable short range predictor, and convergence at a boundary would be especially intriguing. Figure 19 shows the composite frequency out of a total of about 4000 observations that reported 1.27 cm or more of measured rainfall between 1800 and 0000 GMT displayed spatially with respect to a point where there was a moisture convergence maximum along a wet bulb potential temperature boundary. The diagram is oriented such that the wet bulb potential temperature gradient points to the top and thus the down-shear direction is to the right. The sample frequency of heavy rains was 1.8 percent. Figure 19 shows that when a moisture convergence maximum is diagnosed along boundary, frequencies greater than 100% above sample frequency are found just to the warm side and downshear of the diagnosed point, as well as immediately downshear, in the 3-9 h subsequent period, if 1500 GMT surface reports are employed. Further, locations upshear and into the "cold" air have frequencies of heavy rain that ran about half of the sample climatology. Further analysis showed that about 70% of the upshear cases occurred when there was warm advection on the "cold" side of the boundary, implying that forecasters might be able to discriminate the pattern even further.

Analysis of numerous other fields and of the general behavior of the moisture divergence suggest, from this sample, that values of moisture divergence less than $-12 \times 10^{-5} g \ kg^{-1}s^{-1}$ at 1500 GMT and any decline in sea-level pressure reported between 1200 GMT and 1500 GMT (a time of normal rises) are associated with substantially above-climatology heavy rainfalls; conversely, rising pressures, weak moisture convergences, or divergences were associated with below sample climatology heavy rain frequencies.
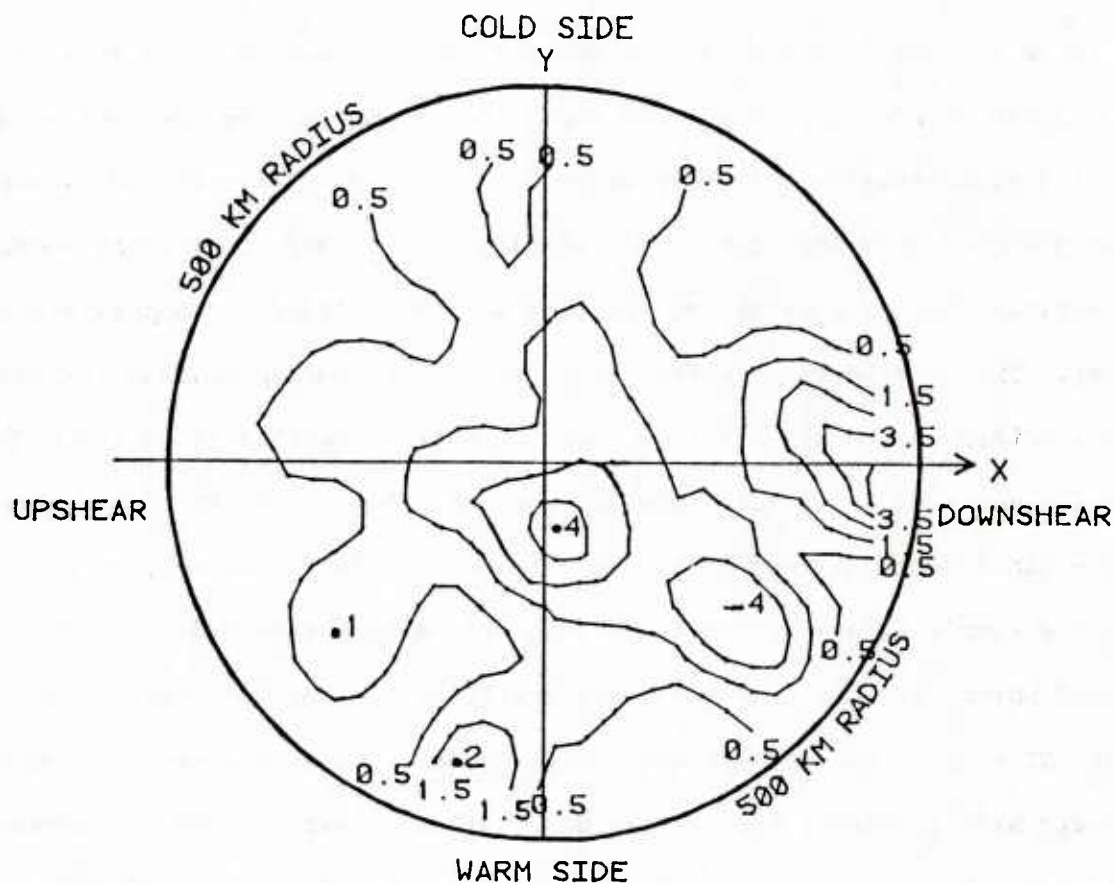
Figure 19.   Composite frequency of 1.27 cm rains in subsequent 3-9 h expressed as a function of distance from a moisture convergence point along a boundary (center of diagram). Total sample frequency was 1.6 percent observations having 1.27 cm or more. Surface wet bulb potential temperature gradient is directed toward top of diagram.

The pilot study suggests that short-range forecasting models based on mesoscale wind, moisture (especially in lower levels) and pressure observations may have substantial promise for a very difficult problem.

V. Conclusions

The work reported here consists of three main results, all of which relate to the perplexing problem of inferring the behavior of the moisture field--the object of many weather forecasts--for application over short time ranges and small space scales. Many, if not most, interesting forecasting situations occur in cloudy regions, where current and most proposed remote sensing techniques fail. Thus, we have developed a model of the moist conveyor belt which reveals some details of its wind and humidity structure. We have developed and tested a technique for diagnosing, locating and displaying potentially active surface boundaries. We have tested its application in real-time conditions, and performed a pilot study to extend it into an objective aid in short-term (3-9 h) prediction of strong rains. Also, we have identified a method of classifying polar lows, and recognizing the satellite indicators of strong ones. Further, we have identified the larger-scale conditions favorable for their growth.

All of these approaches can generate only very small gains in forecasting skill, at best, as our experiments show. But they do lend insight into what can be done over the next few years as mesoscale wind observations become available. The work also suggests that short range forecasting is limited by inadequate moisture observations and that a major effort is needed in that area.

References

Bosart, L.F., 1970: Mid-tropospheric frontogenesis. Quart. J. Roy. Meteor. Soc., 96, 442-471.

Browning, K.A. and T.W. Harrold, 1969: Air motion and precipitation growth in a wave depression. Quart. J. Roy. Meteor. Soc., 95, 288-309.

Browning, K.A., 1971: Radar measurements of air motion near fronts. Weather, 26, 288-309.

Carlson, T.N., 1980: Airflow through midlatitude cyclones and the comma cloud pattern. Mon. Wea. Rev., 108, 1498-1509.

Clarke, L.C. and R.J. Renard, 1966: The U.S. Navy numerical frontal analysis scheme: Further development and a limited evaluation. J. Appl. Meteor., 5, 764-777.

Dvorak, V.F., 1975: Tropical cyclone intensity analysis and forecasting from satellite imagery. Mon. Wea. Rev., 103, 420-430.

Eliassen, A., 1962: On the vertical circulation in frontal zones. Geofys. Publ., 24, 147-160.

Emanuel, K.A., 1979: Inertial instability and mesoscale convective systems. Part I: Linear theory of inertial instability in rotating, viscous systems. J. Atmos. Sci., 36, 2425-2449.

Forbes, G.S., T.A. Paone, and J.J. Cahir, 1982: A minicomputer objective scheme for short-range forecasting of mesoscale convection patterns. Preprints, 12th AMS Conf. on Severe Local Storms, San Antonio, TX.

Fujita, T.T., 1963: Analytical mesometeorology: A review. Meteor. Monographs, 5, 77-125.

Harrold, T.W., 1973: Mechanisms influencing the distribution of precipitation within baroclinic disturbances. Quart. J. Roy. Meteor. Soc., 99, 232-351.

Hjelmfelt, M.R., W.A. Lyons, and R.A. Pielke, 1983: Mesoscale spiral vortex embedded within a Lake Michigan snow squall band: Observations and simulation. Oral presentation, 1st Mesoscale Conf., Norman, OK.

Hoskins, B.J., 1971: Atmospheric frontogenesis models: Some solutions. Quart. J. Roy. Meteor. Soc., 97, 139-153.

Hoskins, B.J., I.Draghici, and H.C. Davies, 1978: A new look at the ω-equation. Quart. J. Roy. Meteor. Soc., 104, 31-38.

Hoskins, B.J. and N.V. West, 1979: Baroclinic waves and frontogenesis. Part II: Uniform potential vorticity jet flows-cold and warm fronts. J. Atmos. Sci., 36, 1663-1680.

Huber-Pock, F. and C. Kress, 1981: Contributions to the problem of numerical frontal analysis. Proc. of the Symp. on Current Probs. of Wea. Pred., Vienna, Austria, June 23-26, 1981. Publ. No. 253, Zentralansradt fur Meteorologie und Geodynamik.

Junker, N.W. and D.J. Haller, 1980: Estimation of surface pressures by satellite cloud pattern recognition. Preprints, 8th Conf. Wea. Forecasting and Analysis, Denver, Amer. Meteor. Soc., 119-122.

Lyall, I.T., 1972: The polar low over Britain. Weather, 27, 378-390.

Maddox, R.A., 1980: Mesoscale convective complexes. Bull. Amer. Meteor. Soc., 61, 1374-1387.

Monteverdi, J.P., 1976: The single air mass disturbance and precipitation characteristics at San Francisco. Mon. Wea. Rev., 104, 1289-1296.

Mullen, S.L., 1979: An investigation of small synoptic-scale cyclones in polar airstreams. Mon. Wea. Rev., 107, 1636-1647.

Namias, J. and P.F. Clapp, 1949: Confluence theory of the high tropospheric jet stream. J. Meteor., 6, 330-336.

Oerlemans, J., 1980: A case study of a subsynoptic disturbance in a polar outbreak. Quart. J. Roy. Meteor. Soc., 106, 313-325.

Oliver, V.J., R.K. Anderson, and E.W. Ferguson, 1964: Some examples of the detection of jet streams from TIROS photographs. Mon. Wea. Rev., 92, 441-448.

Purdom, J.F.W., 1976: Some uses of high resolution GOES imagery in the mesoscale forecasting of convection and its behavior. Mon. Wea. Rev., 104, 1474-1483.

Rasmussen, E., 1979: The polar low as an extratropical CISK disturbance. Quart. J. Roy. Meteor. Soc., 105, 531-549.

Reed, R.J., 1979: Cyclogenesis in polar airstreams. Mon. Wea. Rev., 107, 38-52.

Sardie, J.M. and T.T. Warner, 1983: On the mechanism for the development of polar lows. J. Atmos. Sci., 40, 869-881.

Sawyer, J.S., 1956: The vertical circulation of meteorological fronts and its relation to frontogenesis. Proc. Roy. Soc. London, A234, 346-362.

Seaman, N.L., H. Otten, and R.A. Anthes, 1982: A rapidly developing polar low in the North Sea on January 2, 1979. Preprints, 1st Int'l. Conf. on Meteor. and Air/Sea Interaction of the Coastal Zone. The Hague, Netherlands, Amer. Meteor. Soc., 196-203.

Shapiro, M.A., 1981: Frontogenesis and geostrophically-forced secondary circulations in the vicinity of jet stream-frontal zone systems. J. Atmos. Sci., 38, 954-973.

Uccellini, L.W. and D.R. Johnson, 1979: The coupling of upper and lower tropospheric jet streaks and implications for the development of severe convective storms. Mon. Wea. Rev., 107, 682-703.

Weldon, R., 1979: Cloud patterns and the upper air wind field. U.S. Air Force, Air Weather Service, AWS/TR-79-003, 80 pp. Available from NTIS [ADA-099155].

COMMANDER IN CHIEF
U.S. ATLANTIC FLEET
ATTN: NSAP SCIENCE ADVISOR
NORFOLK, VA 23511

CINCUSNAVEUR
ATTN: NSAP SCIENCE ADVISOR
BOX 100
FPO NEW YORK 09501

COMSECONDFLT
ATTN: NSAP SCIENCE ADVISOR
FPO NEW YORK 09501-6000

COMTHIRDFLT
ATTN: NSAP SCIENCE ADVISOR
PEARL HARBOR, HI 96860

COMSEVENTHFLT
ATTN: NSAP SCIENCE ADVISOR
BOX 167
FPO SEATTLE 98762

COMSIXTHFLT/COMFAIRMED
ATTN: NSAP SCIENCE ADVISOR
FPO NEW YORK 09501-6002

COMMANDER NAVAL AIR FORCE
U.S. ATLANTIC FLEET
ATTN: NSAP SCIENCE ADVISOR
NORFOLK, VA 23511

COMNAVAIRPAC
ATTN: NSAP SCIENCE ADVISOR
NAS, NORTH ISLAND
SAN DIEGO, CA 92135

COMNAVSURFLANT
ATTN: NSAP SCIENCE ADVISOR
NORFOLK, VA 23511

COMNAVSURFPAC
(OO5/N6N)
ATTN: NSAP SCIENCE ADVISOR
SAN DIEGO, CA 92155

COMSUBFORLANT
ATTN: NSAP SCI. ADV. (013)
NORFOLK, VA 23511

ASST. FOR ENV. SCIENCES
ASST. SEC. OF THE NAVY (R&D)
ROOM 5E731, THE PENTAGON
WASHINGTON, DC 20350

CHIEF OF NAVAL RESEARCH (2)
LIBRARY SERVICES, CODE 784
BALLSTON TOWER #1
800 QUINCY ST.
ARLINGTON, VA 22217

OFFICE OF NAVAL RESEARCH
CODE 422AT
ARLINGTON, VA 22217

OFFICE OF NAVAL RESEARCH
CODE 420
ARLINGTON, VA 22217

OFFICE OF NAVAL RESEARCH
CODE 422
ARLINGTON, VA 22217

OFFICE OF NAVAL RESEARCH
CODE 422 PO
ARLINGTON, VA 22217

OFFICE OF NAVAL RESEARCH
CODE 422 MM
ARLINGTON, VA 22217

CHIEF OF NAVAL OPERATIONS
(OP-952)
U.S. NAVAL OBSERVATORY
WASHINGTON, DC 20390

CHIEF OF NAVAL OPERATIONS
NAVY DEPT. OP-986G
WASHINGTON, DC 20350

CHIEF OF NAVAL OPERATIONS
U.S. NAVAL OBSERVATORY
DR. R. W. JAMES, OP-952D1
34TH & MASS. AVE., NW
WASHINGTON, DC 20390

SUPERINTENDENT
LIBRARY REPORTS
U.S. NAVAL ACADEMY
ANNAPOLIS, MD 21402

DIRECTOR OF RESEARCH   (2)
U.S. NAVAL ACADEMY
ANNAPOLIS, MD 21402

NAVAL POSTGRADUATE SCHOOL
METEOROLOGY DEPT.
MONTEREY, CA 93943

LIBRARY
NAVAL POSTGRADUATE SCHOOL
MONTEREY, CA 93943

COMMANDER   (2)
NAVAIRSYSCOM
ATTN: LIBRARY (AIR-7226)
WASHINGTON, DC 20361

COMMANDER
NAVAIRSYSCOM (AIR-330)
WASHINGTON, DC 20361

USAFETAC/TS
SCOTT AFB, IL 62225

AFGL/LY
HANSCOM AFB, MA 01731

AFGL/OPI
HANSCOM AFB, MA 01731

COMMANDING OFFICER
U.S. ARMY RESEARCH OFFICE
ATTN: GEOPHYSICS DIV.
P.O. BOX 12211
RESEARCH TRIANGLE PARK, NC
    27709

DIRECTOR   (12)
DEFENSE TECH. INFORMATION
    CENTER, CAMERON STATION
ALEXANDRIA, VA 22314

HEAD, ATMOS. SCIENCES DIV.
NATIONAL SCIENCE FOUNDATION
1800 G STREET, NW
WASHINGTON, DC 20550

LABORATORY FOR ATMOS. SCI.
NASA GODDARD SPACE FLIGHT CEN.
GREENBELT, MD 20771

COLORADO STATE UNIVERSITY
ATMOSPHERIC SCIENCES DEPT.
ATTN: DR. WILLIAM GRAY
FORT COLLINS, CO 80523

CHAIRMAN
INSTITUTE OF ATMOS. PHYSICS
UNIV. OF ARIZONA
TUSCON, AZ 85721

SCRIPPS INSTITUTION OF
    OCEANOGRAPHY, LIBRARY
DOCUMENTS/REPORTS SECTION
LA JOLLA, CA 92037

ATMOSPHERIC SCIENCES DEPT.
UCLA
405 HILGARD AVE.
LOS ANGELES, CA 90024

CHAIRMAN, METEOROLOGY DEPT.
UNIVERSITY OF OKLAHOMA
NORMAN, OK 73069

CHAIRMAN, METEOROLOGY DEPT.
CALIFORNIA STATE UNIVERSITY
SAN JOSE, CA 95192

COLORADO STATE UNIVERSITY
ATMOSPHERIC SCIENCES DEPT.
ATTN: LIBRARIAN
FT. COLLINS, CO 80523

UNIVERSITY OF WASHINGTON
ATMOSPHERIC SCIENCES DEPT.
SEATTLE, WA 98195

CHAIRMAN, METEOROLOGY DEPT.
PENNSYLVANIA STATE UNIV.
503 DEIKE BLDG.
UNIVERSITY PARK, PA 16802

FLORIDA STATE UNIVERSITY
ENVIRONMENTAL SCIENCES DEPT.
TALLAHASSEE, FL 32306

UNIVERSITY OF HAWAII
METEOROLOGY DEPT.
2525 CORREA ROAD
HONOLULU, HI 96822

DIRECTOR
COASTAL STUDIES INSTITUTE
LOUISIANA STATE UNIVERSITY
ATTN: O. HUH
BATON ROUGE, LA 70803

ATMOSPHERIC SCIENCES DEPT.
OREGON STATE UNIVERSITY
CORVALLIS, OR 97331

UNIVERSITY OF MARYLAND
METEOROLOGY DEPT.
COLLEGE PARK, MD 20742

CHAIRMAN
ATMOS. SCIENCES DEPT.
UNIVERSITY OF VIRGINIA
CHARLOTTESVILLE, VA 22903

CHAIRMAN
METEOROLOGY DEPT.
MASSACHUSETTS INSTITUTE OF
   TECHNOLOGY
CAMBRIDGE, MA 02139

CHAIRMAN, METEOROLOGY DEPT.
UNIVERSITY OF UTAH
SALT LAKE CITY, UT 84112

CHAIRMAN
METEOROLOGY & OCEANO. DEPT.
UNIVERSITY OF MICHIGAN
4072 E. ENGINEERING BLDG.
ANN ARBOR, MI 48104

TEXAS A&M UNIVERSITY
METEOROLOGY DEPT.
COLLEGE STATION, TX 77843

ATMOSPHERIC SCIENCES CENTER
DESERT RESEARCH INSTITUTE
P.O. BOX 60220
RENO, NV 89506

ATMOSPHERIC SCI. RSCH. CENTER
NEW YORK STATE UNIV.
1400 WASHINGTON AVE.
ALBANY, NY 12222

BUREAU OF METEOROLOGY
BOX 1289K, GPO
MELBOURNE, VIC, 3001
AUSTRALIA

METEORO. OFFICE LIBRARY
LONDON ROAD
BRACKNELL, BERKSHIRE
REG 12 1SZ, ENGLAND

U216715